WILEY-VCH

DOI: 10.1002/((please add manuscript number))
Article type: Communication

Tailor-Made Microporous Metal-Organic Frameworks for the Full Separation of Propane from Propylene Through Selective Size Exclusion

*Hao Wang, Xinglong Dong, Valentina Colombo, Qining Wang, Yanyao Liu, Wei Liu, Xin-Long Wang, Xiao-Ying Huang, Davide M. Proserpio, Angelo Sironi, Yu Han, and Jing Li**

Dr. H. Wang, Q.N. Wang, Y.Y. Liu, Prof. J. Li
Department of Chemistry and Chemical Biology
Rutgers University
610 Taylor Road, Piscataway, NJ, 08854, USA
Email: jingli@rutgers.edu
Dr. X.L. Dong, Prof. Y. Han
Advanced Membranes and Porous Materials Center
Physical Sciences and Engineering Division
King Abdullah University of Science and Technology
Thuwal 23955-6900, Kingdom of Saudi Arabia
Dr. V. Colombo, Prof. D.M. Proserpio, Prof. A. Sironi
Dipartimento di Chimica
Università degli Studi di Milano
20133 Milano, Italy
Prof. X.-L. Wang
Department of Chemistry
Northeast Normal University
Changchun 130024, Jilin, China
Prof. X.-Y. Huang
State Key Laboratory of Structural Chemistry
Fujian Institute of Research on the Structure of Matter
the Chinese Academy of Sciences Fuzhou
Fujian, 350002, P.R. China
Dr. H. Wang, Dr. W. Liu, Prof. J. Li
Hoffmann Institute of Advanced Materials
Shenzhen Polytechnic
Xili, Nanshan, Shenzhen 518055, China
Prof. D.M. Proserpio
Samara Center for Theoretical Materials Science
Samara State Technical University
Samara 443100, Russia

Keywords: metal-organic frameworks, adsorbent, adsorptive separation, olefin/paraffin separation, molecular sieving

Abstract: Adsorptive separation of olefin/paraffin mixtures by porous solids could greatly reduce the energy consumption associated with the currently employed cryogenic distillation technique. Here we report the complete separation of propane and propylene by a designer microporous metal-organic framework (MOF) material. The compound, $Y_6(OH)_8(abtc)_3(H_2O)_6(DMA)_2$ (Y-abtc, abtc = 3,3',5,5'-azobenzene-tetracarboxylates, DMA = dimethylammonium), is rationally designed through topology-guided replacement of inorganic building units. Y-abtc is both thermally and hydrothermally robust, and possesses optimal pore window size for propane/propylene separation. It adsorbs propylene with fast kinetics under ambient temperature and pressure, but fully excludes propane, as a result of selective size exclusion. Multicomponent column breakthrough experiments confirm polymer-grade propylene (99.5%) can be obtained by this process, demonstrating its true potential as an alternative sorbent for efficient separation of propane/propylene mixtures.

Olefin/Paraffin separation, listed among the "seven chemical separations to change the world",[1] is of high commercial importance as highly pure olefins (e.g. propylene and ethylene) are required to comply "polymer-grade" specifications for the manufacture of plastics. The separation is, however, particularly difficult to accomplish because of the close volatilities of the components.[2] Propylene is one of the most important olefins in petrochemical industry, primarily because of its use in the production of polypropylene, the world's second-most widely produced synthetic plastic. The global demand for polypropylene has been rising continuously and its annual growth rate is expected to be 4-5% before 2020, resulting in increasing need for polymer-grade (> 99.5 %) propylene.[3] Nevertheless, the production of highly pure propylene represents a challenging and complicated process, which involves the separation of propylene from a propane/propylene mixture. Propane/propylene mixtures are typically obtained by steam cracking of naphtha or during fluid catalytic cracking of gas oils in refineries, with a propylene purity of 50-60% for the former and 80-87% for the latter. Conventional separation of propane

and propylene relies on cryogenic distillation, which is carried out at about 243 K and 0.3 MPa in a column containing over 100 trays.[4] Undoubtedly, this heat-driven process is highly energy-intensive.

To lower the energy and operational cost and to suppress the carbon emissions associated with the propylene purification process through cryogenic distillation, several alternative technologies have been proposed and among them, adsorptive separation, such as pressure/temperature swing adsorption and gas phase simulated moving bed have demonstrated great promise and can potentially offer higher energy efficiency.[3] In this context, the development of a suitable adsorbent is of paramount importance for successful implementation of the adsorptive separation technology. To this end, a wide variety of porous solids have been examined for the separation of propane and propylene, including silica-gel,[5] zeolites,[6-7] and carbon molecular sieves[8] to name a few. However, these materials have yet to meet the stringent requirement for industrial implementation, and thus, search for ideal adsorbents remains ongoing.

The newly emerged family of crystalline sorbent materials, metal-organic frameworks (MOFs),[9-12] hold particular promise for hydrocarbon separation including paraffin/olefin separation in light of their tunable pore size, pore shape, and surface functionality.[13-17] Long and coworkers demonstrated that MOFs with open metal sites show favorable adsorption toward olefins over paraffins as a result of a side-on coordination of olefins at the unsaturated metal centers.[18-19] Thus, this type of MOF materials, analogous to π-complexation zeolites/mesoporous silica,[20-21] are capable of discriminating multiple olefins (e.g. ethylene + propylene) from paraffins through thermodynamically-driven separation. On the other hand, in the case of propane/propylene separation, where the removal of a single olefin from its corresponding paraffin is needed, kinetically-driven separation often proves to be more suitable and efficient.[3] A number of adsorbents have been reported to undergo kinetic separation toward propane and propylene.[22-24] Compared to conventional adsorbents, the MOF pore size

can be tuned much more readily to achieve significantly improved performance for kinetic separation of the two C3 molecules, as demonstrated in several recent studies.[15, 24] The third separation mechanism is based on selective size exclusion where one adsorbate is adsorbed while the other is completely excluded. This mechanism is considered an ideal scenario for gas separation as it offers the highest separation selectivity among three different mechanisms.[15, 25] A widely studied example is Zeolite 4A[26-27] as it selectively adsorbs propylene but excludes propane. However, its adsorption kinetics for propylene is very slow, resulting in poor separation performance under mixed-gas conditions.[15]

Herein, we show that Y-abtc, a microporous metal-organic framework material with cage-like pores, exhibits fast and complete separation of propane/propylene mixtures through selective molecular exclusion mechanism. The optimal pore structure of this material is achieved by a topology-guided design strategy, which involves the precise tuning of pore aperture by judicious selection of structure topology, inorganic nodes and organic linkers. Like zeolite 4A, Y-abtc adsorbs propylene but fully excludes propane, yet it is superior to zeolite 4A as it exhibits a much faster adsorption kinetics for propylene. Multicomponent column breakthrough measurements demonstrate that Y-abtc is capable of producing propylene with a purity of 99.5% from a typical mixture concentration of cracking product, meeting the "polymer grade" specification required for the production of polypropylene. This structure, built on hexanuclear Y6 clusters, exhibits high thermal and hydrothermal stability. In addition, its synthesis is facile and can be easily scaled up. It should be noted that during the preparation of this manuscript, Eddaoudi et al. reported a similar structure built on Tb and abtc, which shows kinetic separation rather than selective size exclusion toward propane and propylene.[28] In light of its attractive structural features, fast adsorption kinetics and highest selectivity for propylene over propane, we believe Y-abtc represents a notable advancement for the adsorptive separation of the C3 paraffin and olefin, and holds strong promise for industrial implementation. Furthermore, the material design strategy presented here may offer guidance for further

research and advancement in developing MOFs with suitable pore structure for industrially challenging molecular separations.

We recently reported topology-guided construction of Zr-MOFs built on tetratopic carboxylate linkers and their uses for the separation of C6 alkane isomers.[29] As Zr_6O_8 building block is commonly adopted in Zr-MOFs, their structural topology, depending on the connectivity of the Zr6 cluster and the geometry of the organic linker, is generally predictable or designable by making use of reticular chemistry. Three different structures with **ftw**, **scu**, and **lvt** topology were obtained and the connectivity of the Zr6 cluster and the topology of the resulting Zr-MOFs are closely related to the shape (i.e. aspect ratio) of the organic linker. The use of the smallest linker bptc led to the formation of a **ftw** type structure with 12-connected Zr6 cluster (Zr-bptc). Structures with **ftw** topology are particularly favorable for molecular separation as they feature large cages connected through small windows.[30] The pore aperture is mainly regulated by the size of the organic linker (i.e. distance between adjacent carboxylates). Zr-bptc shows optimal pore aperture for the separation of alkane isomers as it adsorbs linear alkanes only and excludes any branched isomers. With this in mind, it is reasonable to speculate that a similar structure with slightly reduced size of pore window may be suitable for discriminating linear paraffins and olefins such as propane and propylene. However, in practice, this is difficult to achieve by replacing bptc with an even shorter ligand. This is because bptc, comprised of two isophthalates, may be the smallest organic linker suited for the construction of **ftw** type structure. An alternative approach is to explore the possibility of modifying the inorganic building unit while maintaining the overall connectivity and topology. A careful screening analysis suggests that Y6 cluster, which resembles the Zr6 cluster with respect to composition, geometry, and connectivity, may be a good choice.[31-32] Reported by Eddaoudi and coworkers,[33] Y6 cluster connects to carboxylate linkers in a similar fashion as that of Zr6 in Zr-MOFs, and forms structures with identical topology to that of the latter with the same organic linkers (**Figure 1**). Nevertheless, due to the negative charge of the 12-

connected cluster $[Y_6(OH)_8(H_2O)_6(COO)_{12}]^{2-}$ and the propagated framework, balancing cations (usually dimethylammonium, assuming N,N-dimethylformamide is the solvent used for synthesis) are present in the structure, which can potentially act as a regulatory factor to fine control and adjust pore dimensions.[34] For a given organic linker, the presence of charge balancing cations in the Y6 based MOF may slightly reduce the effective pore size compared to its analogous structure built on Zr6 cluster. This prompted us to explore the possibility of replacing Zr6 clusters in the aforementioned Zr-MOFs by Y6 cluster, thus fine-tuning the pore size of MOFs for the separation of propane and propylene.

Our initial attempt started with the synthesis of Y-MOF with H_4bptc, aiming at a **ftw** structure analogous to Zr-bptc but with slightly smaller pore aperture in hope that the resultant structure may be suitable for the target separation of propane and propylene. Colorless cubic crystals of Y-bptc was successfully obtained via solvothermal reactions of $Y(NO_3)_3 \cdot 6H_2O$ and H_4bptc in a mixed solvent of DMF and water, using 2-fluorobenzoic acid as an acidic modulator (Figure S1).[35] Single crystal X-ray diffraction analysis reveals that Y-bptc crystallizes in the cubic *Im-3* space group. As expected, the structure is built on 12-connected $[Y_6(OH)_8(H_2O)_6(COO)_{12}]^{2-}$ SBU with six Y^{3+} ions assembled into an octahedron where μ_3-OH^- anions occupy the eight facets of the octahedron (Figure S2). Each Y^{3+} ion is nine coordinated, connecting to four oxygen atoms from four different carboxylate groups, four bridging μ_3-OH^- anions, and one terminal water molecule. The inorganic cluster is slightly different from the commonly observed 12-connected $Zr_6O_4(OH)_4(COO)_{12}$. Due to the lower positive charge of Y^{3+} compared to Zr^{4+}, the four bridging μ_3-O^{2-} in Zr-MOFs are replaced by μ_3-OH^- in Y-analogues. The Y6 cluster is negatively charged while the Zr6 cluster is neutral. In addition, each Y^{3+} is coordinated to an additional terminal water, which is not observed for Zr-based structures. Despite of these differences, the overall connectivity of Y-bptc is identical to that of Zr-bptc, forming the expected **ftw** type structure. Thus it also contains cubic cage-like pores with Y6 clusters on the vertices and $bptc^{4-}$ linkers on the faces, and the cages are interconnected

through small windows (**Figure 1**). While preparing this manuscript we noted a report of the same structure appeared very recently.[28] The phase purity of Y-bptc was confirmed by powder X-ray diffraction analysis (Figure S3).

As will be explained in the following sections, while we demonstrate the pore size of Y-bptc can indeed be effectively reduced with respect to Zr-bptc as a result of topology-directed SBU replacement, such reduction is overly done making the pore window too small to adsorb either propane or propylene. Thus we attempted to further tune the pore size by using a slightly longer organic linker 3,3′,5,5′-azobenzene-tetracarboxylate (H_4abtc) with the Y6 SBU. Solvothermal reactions of $Y(NO_3)_3 \cdot 6H_2O$ and H_4abtc under conditions similar to that of Y-bptc yielded light-yellow, small, block-shaped crystals (Figure S1). Although powder X-ray diffraction patterns indicated its high crystallinity (Figure S4), attempts for determining the structure by single crystal X-ray diffraction analysis didn't succeed. We instead decided to try to retrieve the crystal structure through *ab initio* structure solution methods (See Supporting Information for details).[36-37] Indexing of the powder pattern suggested that Y-abtc, differently from Y-bptc, crystallizes in a rhombohedal rather than a cubic space group. This was eventually confirmed by a successful structure solution (R_p, R_{wp} and R_{Bragg} = 0.0754, 0.1022 and 2.218, respectively, Figure S5) in the *R-3c* space group. The overall connectivity of Y-abtc is identical to that of Y-bptc (**Figure 2**). However, the cages are no longer cubic, because of the rotation of the octahedron driven by the connectivity of the different ligands (Figure S6). As a result, for each face of the cube, in Y-bptc, the plane described by the 4 center of mass of the octahedrons and the one described by the ligand are coincident. For Y-abtc, however, the two planes are not any more coincident and this is due to 1) the mutual rotation of the octahedrons and 2) the coordination geometry of the ligand. The ligand coordination is indeed straight on the Y atom for two COO^- groups and above and below from this plane by the other two COO^- groups (Figure S7). This gives rise to the contraction and distortion of the cage. It should be noted that Y-abtc adopts a 4,12-c connectivity, which is different from Zr-abtc with 4,8-c connectivity as

a result of the large aspect ratio of abtc^{4-} (**Figure 1**).[29] A recent paper by an IUPAC committee[38] explains the different approaches in the deconstruction of crystalline networks into underlying nets, showing how to deal with structures with polytopic ligands and complex SBUs like our compounds. In the commonly used description[38] ("single node" deconstruction) the SBU is a 12-coordinated node and the ligand 4-c (regardless of the shape) resulting in the 4,12-c **ftw** underlying net. If we use the "all node" deconstruction[37] (called "cluster" in ToposPro) we describe the tetratopic ligand as formed by two 3-c nodes. This allows to consider the shape and orientation of ligand on the underlying net giving three 3,12-c nets derived from 4,12-**ftw**: **ttv**, **kle** and **kxe.**[36] Until recently only 3,12-**kle** was observed for ligand of rectangular shape and symmetry D_{2h}[29] and now also for Y-bptc. The change of the ligand to abtc (lowering the symmetry to C_{2h}) in Y-abtc gave access to the new topology 3,12-**kxe** that differs from 3,12-**kle** for the relative orientations of the ligands as shown in the Figure S8. In the Y-abtc crystal structure the clathrate solvent molecules and the balancing extra-framework cations are disordered into the voids of this MOF. We manage to partly eliminate the solvent by a thermal treatment (see Supplementary Information for details) thus reducing the diffuse electron density in the pores but also increasing the disorder by leaving more 'free room' for the cations and the residual solvent. We estimate that the effect of our description of the diffuse electron density in the 'pores' has the same order of magnitude of the intrinsic inaccuracy of powder data and has little effect on the stereochemistry of the organic-inorganic framework. Indeed, the comparison with the Tb-abtc structure, with which we came across after having solved the Y-abtc structure, confirms that *ab initio* structure solution from powder diffraction data is a truly powerful tool, since the two structural models strongly agrees.

Porosity characterization by N_2 adsorption at 77 K didn't work out for Y-bptc or Y-abtc as neither of them show noticeable uptake of N_2 (Figure S9). This is different from their Zr-based analogues (Zr-bptc and Zr-abtc) which adsorb substantial amount of N_2 at 77 K. A possible reason could be the existence of balancing cations in the Y-based structures, leading to the

suppression of accessible size of pore windows which does not allow the diffusion of N_2 into their pores at cryogenic temperature. We then turned to characterize their porosity by CO_2 adsorption at 195 K. Y-bptc and Y-abtc both exhibit Type I adsorption profile for CO_2, with saturation capacities of 3.2 and 3.7 mmol g^{-1}, respectively. The estimated surface areas and pore volumes are 319 and 427 m^2 g^{-1}, and 0.14 and 0.18 cc g^{-1} for Y-bptc and Y-abtc, respectively. These values are noticeably lower than their Zr-based analogues.[29]

Adsorption isotherms of propane and propylene on Zr-bptc and Zr-abtc at room temperature indicate neither of them is capable of discriminating the two gases (**Figure 3**a and **3**b). The adsorption capacity of propane and propylene are similar for both compounds. Besides, no diffusional restriction has been observed. The results suggest that the aperture sizes of Zr-bptc and Zr-abtc are too large for the separation of propane and propylene. In contrast, while Y-bptc features the same connectivity and topology as Zr-bptc, it adsorbs neither propane nor propylene, indicating its pore aperture size is smaller than that of Zr-bptc (**Figure 3**c). This could be attributed to the existence of the balancing cation, dimethylammonium, which might block the entrance of the cage and suppress the effective pore aperture. A more detailed discussion will be presented in the following section.

Unlike Y-bptc, Y-abtc adsorbs appreciable amount of propylene at room temperature, with an uptake capacity of ~ 2 mmol g^{-1} at 1 bar (**Figure 3**d). The adsorption is fully reversible and features a Type I profile. Adsorption isotherms at higher temperatures (40, 60, 80 °C) have also been collected, and at 80 °C propylene adsorption capacity is ~ 1.5 mmol g^{-1} (**Figure 3**e). Adsorption strength has been evaluated by isosteric heat of adsorption (Q_{st}), calculated by adsorption isotherms at 40, 60, and 80 °C and a Q_{st} value of ~50 kJ mol^{-1} was obtained. This value is comparable to M_2(dobdc) (M = Mg, Mn, Fe, Co, Ni, Zn), but slightly lower than that of KAUST-7 (57.4 kJ mol^{-1}).[15, 18] We believe the relatively high adsorption heat of Y-abtc for propylene is a combined effect of pore confinement and interaction at the charge-balancing cationbinding sites. The pore aperture of Y-abtc (4.72 Å, Figure 6d) matches very well with the

kinetic diameter of propylene (4.68 Å), which leads to strong pore confinement effect. This was also observed in the case of KAUST-7 which has a Q_{st} for propylene as high as 57.4 kJ mol^{-1}, because of the perfect match between the sizes of pore aperture and propylene.[15] In addition, the charge-balancing cation dimethylammonium may also contribute to the high adsorption affinity, making the Q_{st} value higher than MOFs having open metal sites..[18] The cation effect has been commonly observed in cation exchanged zeolites,[39] as well as in Tb-abtc which has an adsorption heat of 48.8 kJ/mol obtained from calorimetric measurement. The value agrees well with our result.[28] In contrast, adsorption isotherm at room temperature shows essentially no uptake of propane on Y-abtc, indicating a size-exclusion behavior. To confirm the discrimination toward propane and propylene by Y-abtc is through selective size exclusion rather than kinetic separation and to assess the adsorption kinetics of propylene, adsorption rates of propane and propylene at 25 °C and 80 °C were measured with a gravimetric adsorption analyzer (see Supporting Information for details). As shown in **Figure 3**f, adsorption of propylene reaches equilibrium within 20 and 10 minutes at 25 and 80 °C, respectively, without noticeable diffusional restrictions. On the contrary, negligible uptake of propane has been detected and it shows no difference with respect to adsorption kinetics at 25 and 80 °C. This is consistent with the adsorption isotherms, indicating propane is fully excluded from diffusing into the pore of Y-abtc. These results suggest that Y-abtc represents a rare adsorbent that exhibits selective molecular exclusion behavior for propane over propylene. This observed property of Y-abtc can be attributed to its optimal pore window size (4.72 Å, Figure 6d) which falls between the kinetic diameter of propylene (4.68 Å) and propane (5.1 Å).[40]

To assess the framework robustness of Y-abtc with respect to crystallinity and adsorption performance, stability test was performed with thermal and hydrothermal treatments. *In situ* variable-temperature PXRD analysis shows that the framework remains intact up to 520 °C, temperature at which loss of crystallinity starts to take place (Figure S10). Le Bail refinement and parametric treatment of the VT-PXRD data along the whole range of temperature (RT -

540 °C) shows that during activation the framework undergoes a slight contraction of the unit cell volume of less than 1 % (Figure S11). This result displays that Y-abtc possesses high framework robustness, similar to its Zr-based analogues (Zr-bptc and Zr-abtc). As shown in **Figure 4**, after being heated at 180 °C in open air or in water at 80 °C for 3 days, the crystallinity of Y-abtc was well maintained, as evidenced by the PXRD patterns collected on the samples after treatments. More importantly, their propylene adsorption capacity was also fully retained (**Figure 4**b).

As suggested by the single component adsorption results, Y-abtc exhibits potential of separating propane and propylene through complete sieving. We thus performed multicomponent column breakthrough experiments at room temperature to assess its separation capability under mixed gases conditions. We started with an equimolar binary mixture of propane and propylene and a total flow rate of 1.6 ml min^{-1} as a feed. The breakthrough curve reveals that propane breaks at the very first minute indicating no noticeable retention took place in the column (**Figure 5**a). This is consistent with the single component adsorption result that Y-abtc does not adsorb propane at room temperature. Conversely, propylene, the other component in the mixture does not elute out until the 12^{th} minute, equivalent to a dynamic uptake of 1.26 mmol g^{-1}. This again, coincides with the pure component adsorption results that propylene can freely diffuse into the pore of Y-abtc. Subsequent desorption of the gas retained in the column by heating under helium flow yielded a propylene purity of 97.6 % in the eluted gas (**Figure 5**b). A following breakthrough experiment with an increased flow rate (total flow rate: 4 ml min^{-1}) confirmed the complete separation capability of Y-abtc was fully retained with a retention time of 12.9 minutes per gram of adsorbent for propylene (Figure S12), a value noticeably higher than that of KAUST-7, the MOF material with the best performance reported so far for propane/propylene separation, which has a retention time of 5.7 minutes per gram of adsorbent under the same condition.[15] This indicates the dynamic adsorption capacity of Y-abtc for propylene is more than twice higher than that of KAUST-7. This is a significant

improvement considering its complete sieving nature for the propane/propylene separation, scalable synthesis （Figure S13 and S14）and high stability.

Separation of propane and propylene by cryogenic distillation is particularly energy intensive as the production of polymer-grade propylene with a purity of 99.5% requires distillation tower that contains a large number of theoretical plates and is operated with large reflux/feed ratios with tremendous energy input. Thus production of highly pure propylene by adsorptive separation could largely lower the energy cost associated with the separation process.[3] In this context, we further explored the breakthrough experiments with different propane/propylene starting ratios, i.e. propane:propylene = 10:90, and propane:propylene = 5:95 (Figure S12). Clear separation of propane and propylene with propane breaking first was observed in the breakthrough curves for both feed ratios despite the increase of the concentration of propylene in the mixture. For the measurement starting with a mixture of propane: propylene = 5:95, although propane was also retained in the column for several minutes before breaking due to its low concentration, its adsorbed amount on Y-abtc (~ 2 mg g^{-1}) is negligible (**Figure 5**c). Noticeably, 99.5% pure propylene was recovered during the desorption step, a purity that well meets the requirements for the production of polymers (**Figure 5**d). This confirms that Y-abtc, as an adsorbent for complete sieving of propane from propylene, is capable of producing polymer-grade propylene by adsorptive separation method. As mentioned previously, the recently reported Tb-abtc was also examined for the adsorptive separation of propane and propylene. It adsorbs similar amount of propane and propylene at room temperature but the adsorption kinetics for propane is significantly slower than that of propylene, enabling kinetic-based separation of the two gases by mixed-gas breakthrough experiments.[28] In this work the separation is achieved via a different and more efficient mechanism, namely size exclusion. Y-abtc adsorbs propylene and fully excludes propane. The higher selectivity associated with this mechanism is likely the reason for the higher dynamic

adsorption capacity of Y-abtc (1.26 mmol g^{-1}) than that of Tb-abtc (0.9 mmol g^{-1}) under similar conditions (room temperature and with a feed of C_3H_8/C_3H_6:50/50).

The 4,12-c Y-abtc/Y-bptc are similar to their Zr-based analogue Zr-bptc with respect to overall connectivity and pore structure. However, the subtle difference in their structures lead to their distinct adsorption behaviors. One noticeable difference between them is that the framework of the Y-MOFs are anionic while the Zr-MOFs are neutral. To evaluate how the balancing cations in Y-MOFs may influence their pore apertures and contribute to their adsorption properties, we performed gas adsorption measurements on Y-abtc sample activated at different temperatures. The aforementioned adsorption measurements were performed on Y-abtc activated at 200 °C (Figure S15). ^{1}H NMR spectrum of the digested MOF sample indicates the existence of dimethylammonium in the activated compound (Figure S16). On the other hand, Y-abtc activated at 300 °C shows enhanced adsorption capacity and kinetics toward propylene, compared to that of the sample activated at 200 °C (Figure S17), with propylene adsorbed amount of 3.5 mmol g^{-1} (v.s. 2.0 mmol g^{-1} if activated at 200 °C) at 25 °C and 1 bar. Adsorption rate measurements show the adsorption of propylene reach equilibrium within 10 and 4 minutes at 25 and 80 °C, respectively. Besides, upon activation at 300 °C, Y-abtc can adsorb a substantial amount of propane, through the diffusion rate is relatively slow. These results suggest that the increased activation temperature has noticeably enlarged the pore aperture of Y-abtc. To further confirm this hypothesis, CO_2 adsorption experiments at 195 K were carried out on Y-abtc samples activated at 200 and 300 °C. As expected, the sample activated at 300 °C adsorbs more CO_2 under saturation (**Figure 6**). Pore size distribution analysis confirms its enlarged pore size (4.93 Å) compared to that of the sample activated at 200 °C (4.72 Å). More evidently, the peak associated to dimethylammonium disappears on the ^{1}H NMR spectrum of the sample activated at 300 °C (Figure S16), indicating the decomposition of the organic cation. TG-MS measurement indicates that upon heating to 300 °C the material releases a molecular with a molecular mass of 45, which could be attributed to dimethylamine (Figure S18). This

suggests the decomposition of dimethylammonium cation results in the formation of dimethylamine leaving proton acting as balancing cation. This explains the observed enlarged pore aperture and its adsorption behavior toward propylene and propane. CO_2 adsorption results and pore size distribution analysis on Y-bptc suggest a similar trend. This is interesting and noteworthy as ionic MOF frameworks are quite common and making use of the balancing ionic species as a pore size regulator can potentially be an effective way to develop adsorbents with optimal adsorption/separation performance.

Efficient separation of industrially relevant hydrocarbon mixtures by porous solids could potentially reduce the associated high energy cost, but remains challenging as it has stringent requirements for the adsorbents with respect to their adsorption/separation performance, stability, cost, to name a few. The development of inorganic adsorbents (e.g. zeolites) has led to great advancement of adsorptive separation technology and some excellent candidates have already been implemented for separations in industry. However, due to their limited structure diversity and lack of tunability, the search for novel adsorbents that can address such limitations is much needed and is indeed ongoing. Metal-organic frameworks are advantageous for molecular separation as they offer tremendous tunability in terms of structure, porosity, and functionality. Widely used strategies for tuning the pore structure and functionality of MOFs include reticular expansion/shrinkage by ligand design, pre-synthetic ligand functionalization, and post-synthetic functionalization of organic ligands or metal centers, to mention but a few. In this work, in addition to topologically directed framework expansion/shrinkage, we apply the strategy of SBU replacement to further tune the pore structure and make use of the balancing cations as pore size regulators to achieve optimal pore dimension for targeted hydrocarbon separation. The tailor-made Y-abtc displays efficient separation of propane and propylene through selective molecular exclusion. Moreover, it features high stability and scalable synthesis, rendering it a promising candidate for industrial implementation.

Experimental Section

Synthesis of Y-bptc: $Y(NO_3)_3 \cdot 6H_2O$ (38.3 mg, 0.1 mmol) and 2-fluorobenzoic acid (1.0 g, 4.1 mmol) were dissolved DMF/H_2O (5/2 mL) in a 20 mL glass vial and H_4bptc (16.5 mg, 0.05 mmol) was added to the solution. The mixture was solicated for 5 minutes before being placed in 120 °C oven for 3 days. Colorless cubic crystals were obtained by filtration. The crystals were washed by DMF (3 × 5 mL) and then immersed in 5 mL acetone for one week during which the solvent was replaced twice a day. The solvent-exchanged sample was dried at 200 °C under vacuum to yield activated sample. 50× scaled up synthesis resulted in materials with similar crystallinity.

Synthesis of Y-abtc: $Y(NO_3)_3 \cdot 6H_2O$ (38.3 mg, 0.1 mmol) and 2-fluorobenzoic acid (1.5 g, 6 mmol) were dissolved DMF/H_2O (5/2 mL) in a 20 mL glass vial and H_4abtc (17.5 mg, 0.05 mmol) was added to the solution. The mixture was solicated for 5 minutes before being placed in 120 °C oven for 3 days. Orange cubic crystals were obtained by filtration. The crystals were washed by DMF (3 × 5 mL) and then immersed in 5 mL methanol for one week during which the solvent was replaced twice a day. The solvent-exchanged sample was dried at 200 or 300 °C under vacuum to yield activated sample. 50× scaled up synthesis resulted in material with similar crystallinity.

Crystal data for Y-bptc: Cubic crystal system, space group *Im-3*, a = 25.0883(6) Å, V = 15791.15(65) $Å^3$, Z = 8. ρ_{calc} = 1.46718 $g \cdot cm^{-3}$. CCDC No: 1853121.

Crystal data for Y-abtc: Trigonal crystal system, space group *R-3c*, a = 18.0682(7) Å, c = 45.3244(2) Å, V = 12814(1) $Å^3$, Z = 8. ρ_{calc} = 1.457(3) $g \cdot cm^{-3}$, μ(Cu-K_α) =59.5(2) cm^{-1}. R_p and R_{wp} = 0.0754 and, 0.1022 for 5001 data collected in the 5–105° 2θ range. R_{Bragg} = 2.218. CCDC No.: 1856158.

[CCDC 1853121 and 1856158 contain the supplementary crystallographic data for this paper. These data can be obtained free of charge from The Cambridge Crystallographic Data Centre via www.ccdc.cam.ac.uk/data_request/cif.]

Supporting Information
Supporting Information is available from the Wiley Online Library or from the author.

Acknowledgements
We would like to thank the financial support from the Materials Sciences and Engineering Division, Office of Basic Research Energy Sciences of the U.S. Department of Energy through Grant No. DE-FG02-08ER-46491 for the synthesis, characterization and single-component adsorption work. Y.H. acknowledges the KAUST CCF fund for the breakthrough experiments. The RU team would also like to acknowledge Micromeritics Instrument Corp. for the award of a 3Flex system through its Instrument Grant program. V.C thanks the University of Milan for partial funding through the Development Plan of Athenaeum grant.

Received: ((will be filled in by the editorial staff))
Revised: ((will be filled in by the editorial staff))
Published online: ((will be filled in by the editorial staff))

References

[1] D. S. Sholl, R. P. Lively, *Nature* **2016**, *532*, 435.
[2] J. Padin, S. U. Rege, R. T. Yang, L. S. Cheng, *Chem. Eng. Sci.* **2000**, *55*, 4525.
[3] V. F. D. Martins, A. M. Ribeiro, M. G. Plaza, J. C. Santos, J. M. Loureiro, A. F. P. Ferreira, A. E. Rodrigues, *J. Chromatogr. A* **2015**, *1423*, 136.
[4] S. U. Rege, R. T. Yang, *Chem. Eng. Sci.* **2002**, *57*, 1139.
[5] C. A. Grande, A. E. Rodrigues, *Ind. Eng. Chem. Res.* **2001**, *40*, 1686.
[6] F. A. Da Silva, A. E. Rodrigues, *Ind. Eng. Chem. Res.* **1999**, *38*, 2051.
[7] M. Khalighi, Y. F. Chen, S. Farooq, I. A. Karimi, J. W. Jiang, *Ind. Eng. Chem. Res.* **2013**, *52*, 3877.
[8] X. Ma, S. Williams, X. Wei, J. Kniep, Y. S. Lin, *Ind. Eng. Chem. Res.* **2015**, *54*, 9824.
[9] H. Wang, W. P. Lustig, J. Li, *Chem. Soc. Rev.* **2018**.
[10] H. Furukawa, K. E. Cordova, M. O'Keeffe, O. M. Yaghi, *Science* **2013**, *341*.
[11] O. M. Yaghi, M. O'Keeffe, N. W. Ockwig, H. K. Chae, M. Eddaoudi, J. Kim, *Nature* **2003**, *423*, 705.
[12] H. Wang, W. P. Lustig, J. Li, *Chem. Soc. Rev.* **2018**, *47*, 4729.
[13] L. Bin, W. Hailong, C. Banglin, *Chem. - Asian J.* **2014**, *9*, 1474.
[14] K. Adil, Y. Belmabkhout, R. S. Pillai, A. Cadiau, P. M. Bhatt, A. H. Assen, G. Maurin, M. Eddaoudi, *Chem. Soc. Rev.* **2017**, *46*, 3402.
[15] A. Cadiau, K. Adil, P. M. Bhatt, Y. Belmabkhout, M. Eddaoudi, *Science* **2016**, *353*, 137.
[16] H. Wang, X. Dong, E. Velasco, D. H. Olson, Y. Han, J. Li, *Energy Environ. Sci* **2018**, *11*, 1226.

[17] B. Li, X. Cui, D. O'Nolan, H.-M. Wen, M. Jiang, R. Krishna, H. Wu, R.-B. Lin, Y.-S. Chen, D. Yuan, H. Xing, W. Zhou, Q. Ren, G. Qian, M. J. Zaworotko, B. Chen, *Adv. Mater.* **2017**, *29*, 1704210.
[18] S. J. Geier, J. A. Mason, E. D. Bloch, W. L. Queen, M. R. Hudson, C. M. Brown, J. R. Long, *Chem. Sci.* **2013**, *4*, 2054.
[19] E. D. Bloch, W. L. Queen, R. Krishna, J. M. Zadrozny, C. M. Brown, J. R. Long, *Science* **2012**, *335*, 1606.
[20] A. van Miltenburg, J. Gascon, W. Zhu, F. Kapteijn, J. A. Moulijn, *Adsorption* **2008**, *14*, 309.
[21] C. A. Grande, N. Firpo, E. Basaldella, A. E. Rodrigues, *Adsorption* **2005**, *11*, 775.
[22] J. Peng, H. Wang, D. H. Olson, Z. Li, J. Li, *Chem. Commun.* **2017**, *53*, 9332.
[23] K. Li, D. H. Olson, J. Seidel, T. J. Emge, H. Gong, H. Zeng, J. Li, *J. Am. Chem. Soc.* **2009**, *131*, 10368.
[24] C. Y. Lee, Y.-S. Bae, N. C. Jeong, O. K. Farha, A. A. Sarjeant, C. L. Stern, P. Nickias, R. Q. Snurr, J. T. Hupp, S. T. Nguyen, *J. Am. Chem. Soc.* **2011**, *133*, 5228.
[25] Y. Wang, D. Zhao, *Cryst. Growth Des.* **2017**, *17*, 2291.
[26] C. A. Grande, A. E. Rodrigues, *Chem. Eng. Res. Des.* **2004**, *82*, 1604.
[27] M. Khalighi, I. A. Karimi, S. Farooq, *Ind. Eng. Chem. Res.* **2014**, *53*, 16973.
[28] D.-X. Xue, A. Cadiau, L. J. Weselinski, H. Jiang, P. M. Bhatt, A. Shkurenko, L. Wojtas, C. Zhijie, Y. Belmabkhout, K. Adil, M. Eddaoudi, *Chem. Commun.* **2018**, *54*, 6404.
[29] H. Wang, X. Dong, J. Lin, S. J. Teat, S. Jensen, J. Cure, E. V. Alexandrov, Q. Xia, K. Tan, Q. Wang, D. H. Olson, D. M. Proserpio, Y. J. Chabal, T. Thonhauser, J. Sun, Y. Han, J. Li, *Nat. Commun.* **2018**, *9*, 1745.
[30] Y. Bai, Y. Dou, L.-H. Xie, W. Rutledge, J.-R. Li, H.-C. Zhou, *Chem. Soc. Rev.* **2016**, *45*, 2327.
[31] D.-X. Xue, Y. Belmabkhout, O. Shekhah, H. Jiang, K. Adil, A. J. Cairns, M. Eddaoudi, *J. Am. Chem. Soc.* **2015**, *137*, 5034.
[32] V. Guillerm, Ł. J. Weseliński, Y. Belmabkhout, A. J. Cairns, V. D'Elia, Ł. Wojtas, K. Adil, M. Eddaoudi, *Nat. Chem.* **2014**, *6*, 673.
[33] R. Luebke, Y. Belmabkhout, Ł. J. Weseliński, A. J. Cairns, M. Alkordi, G. Norton, Ł. Wojtas, K. Adil, M. Eddaoudi, *Chem. Sci.* **2015**, *6*, 4095.
[34] A. A. H., B. Youssef, A. Karim, B. P. M., X. Dong‐Xu, J. Hao, E. Mohamed, *Angew. Chem. Intl. Ed.* **2015**, *54*, 14353.
[35] R. Luebke, Y. Belmabkhout, L. J. Weselinski, A. J. Cairns, M. Alkordi, G. Norton, L. Wojtas, K. Adil, M. Eddaoudi, *Chem. Sci.* **2015**, *6*, 4095.
[36] C. A. A., *J. Appl. Crystallogr.* **2003**, *36*, 86.
[37] V. A. Blatov, A. P. Shevchenko, D. M. Proserpio, *Cryst. Growth Des.* **2014**, *14*, 3576.
[38] C. Bonneau, M. O'Keeffe, D. M. Proserpio, V. A. Blatov, S. R. Batten, S. A. Bourne, M. S. Lah, J.-G. Eon, S. T. Hyde, S. B. Wiggin, L. Öhrström, *Cryst. Growth Des.* **2018**, *18*, 3411.
[39] B. Demir, M. G. Ahunbay, *Micro. Meso. Mater.* **2014**, *198*, 185.
[40] J.-R. Li, R. J. Kuppler, H.-C. Zhou, *Chem. Soc. Rev.* **2009**, *38*, 1477.

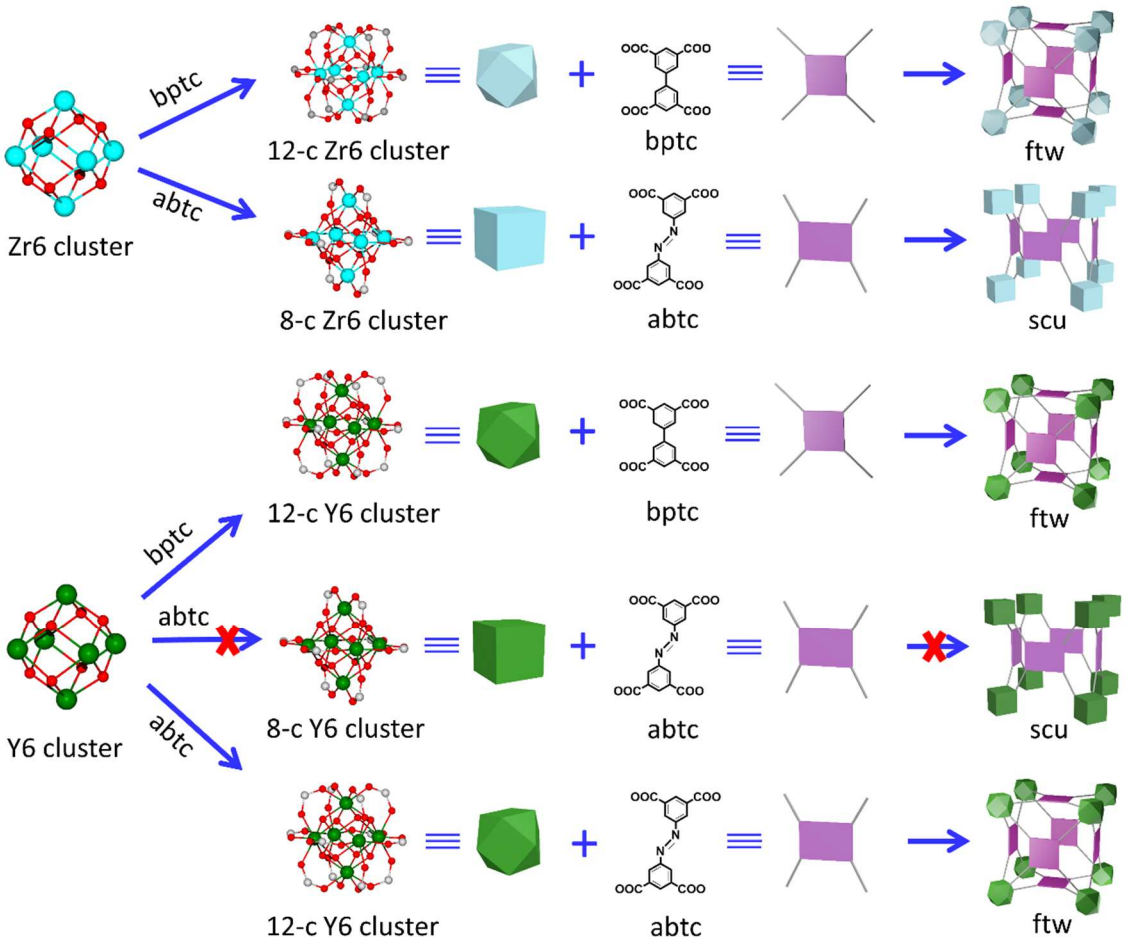

Figure 1. Topology analysis of MOFs built on Zr6/Y6 clusters and two tetratopic linkers. Zr-bptc and Zr-abtc show different connectivity and topology due to the difference of the aspect ratio of organic linkers. Y-bptc and Y-abtc feature similar connectivity and topology to that of Zr-bptc. Hydrogen atoms are omitted for clarity.

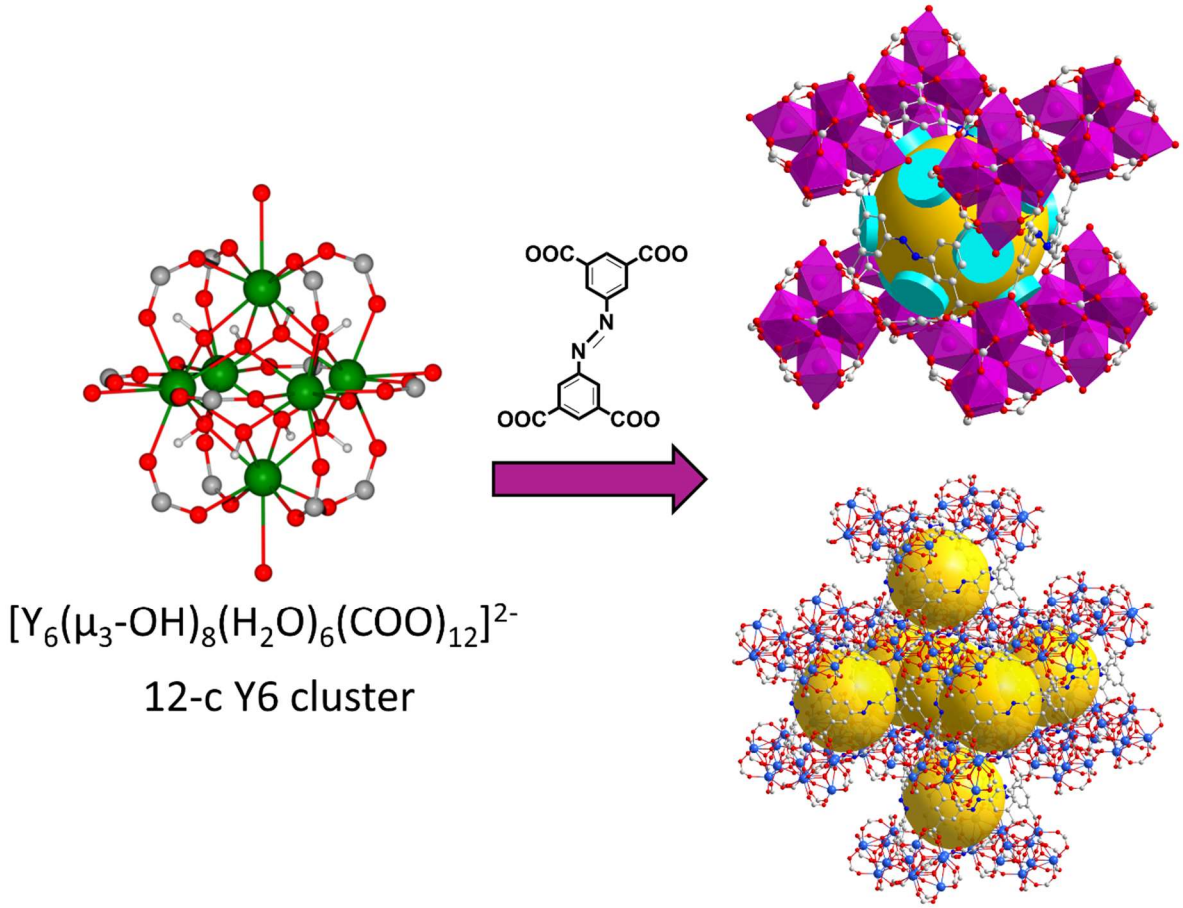

Figure 2. Crystal structure of Y-abtc. Y-abtc is built on 12-connected hexanuclear SBU, forming cage-like pores interconnected by small windows.

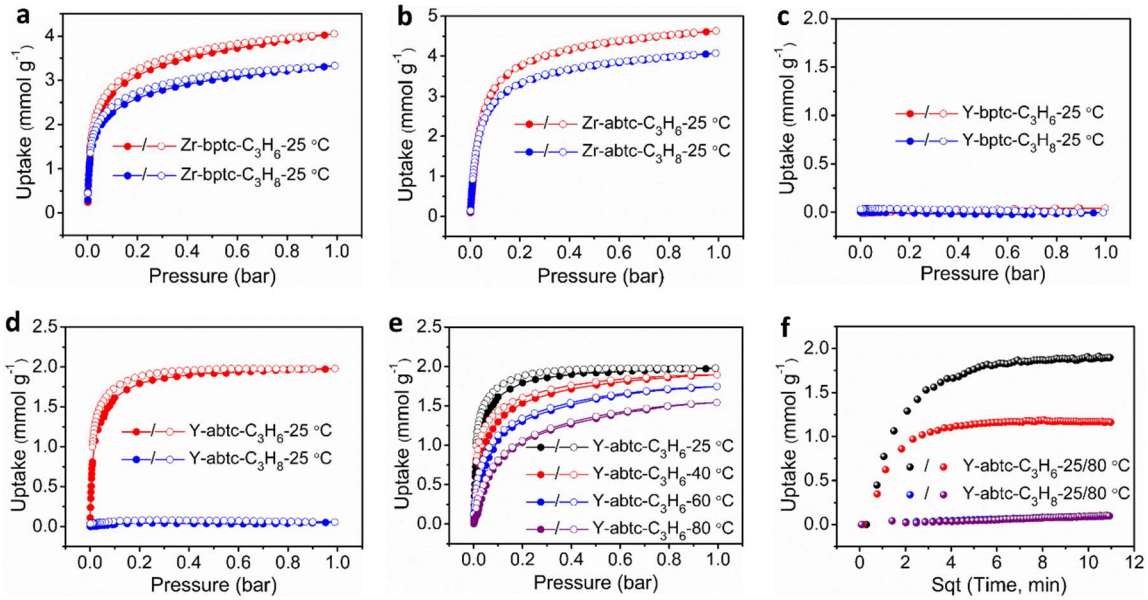

Figure 3. Single-component adsorption results of propane and propylene. Adsorption-desorption isotherms of propane and propylene at 25 °C for a) Zr-bptc, b) Zr-abtc, c) Y-bptc, and d) Y-abtc. e) Propylene adsorption isotherms for Y-abtc at 25, 40, 60, and 80 °C. f) Adsorption rates of propane and propylene on Y-abtc at 25 and 80 °C, with a partial pressure of 0.8 bar.

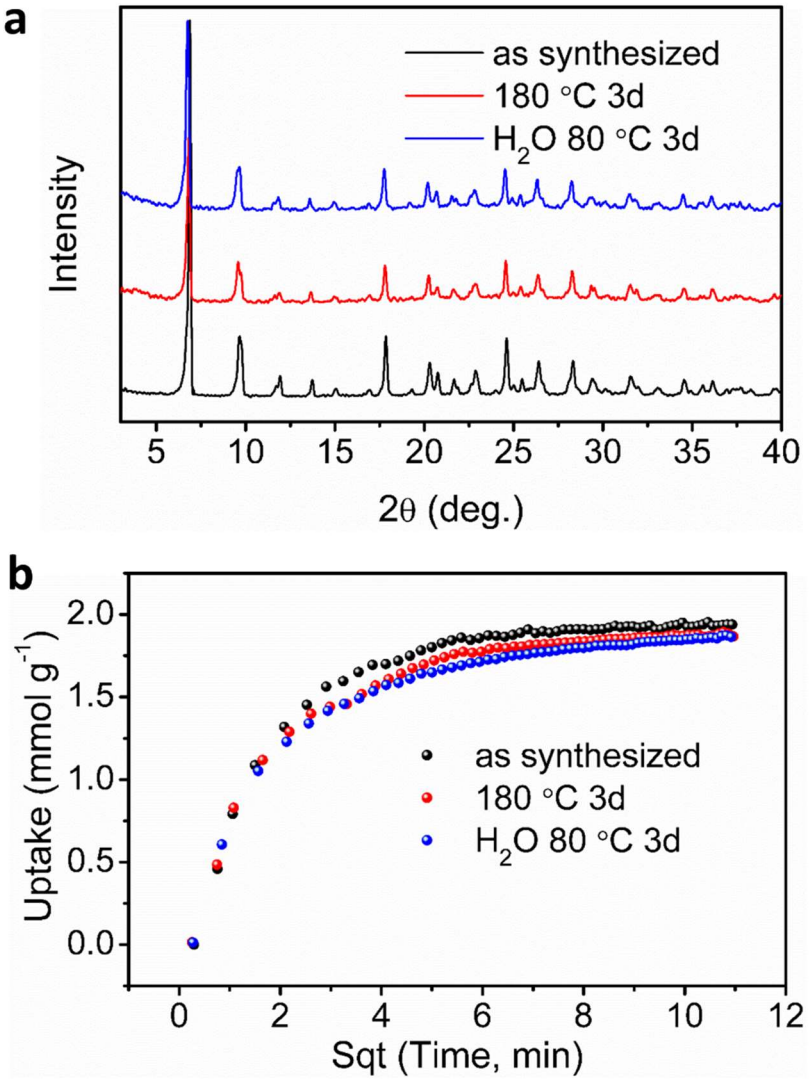

Figure 4. Stability test for Y-abtc. a) Powder X-ray diffraction patterns and b) propylene adsorption for as synthesized Y-abtc and after thermal and hydrothermal treatments.

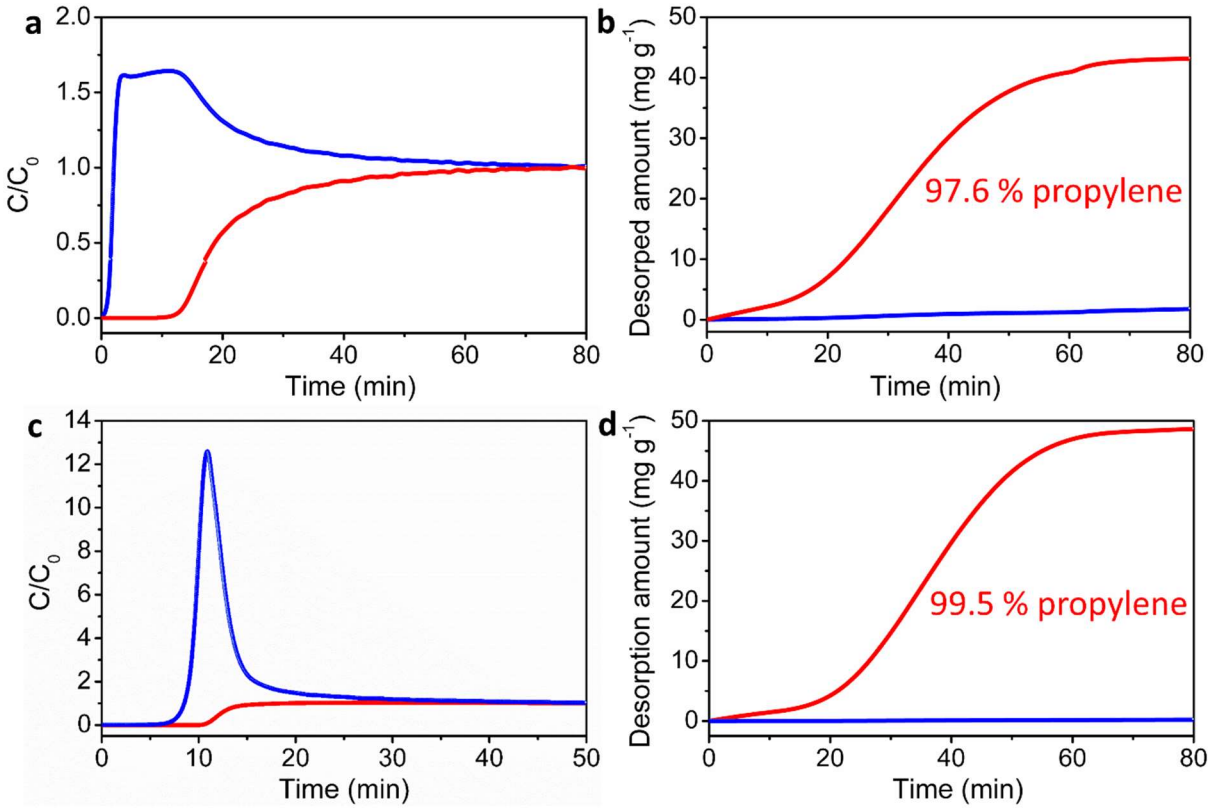

Figure 5. Multicomponent column breakthrough results for Y-abtc at 25 °C. a) Breakthrough curve and b) desorption curve for an equimolar mixture of propane and propylene. c) Breakthrough curve and d) desorption curve for a mixture of propane/propylene with a feed ratio of 5/95. Color scheme: red: propylene, blue: propane.

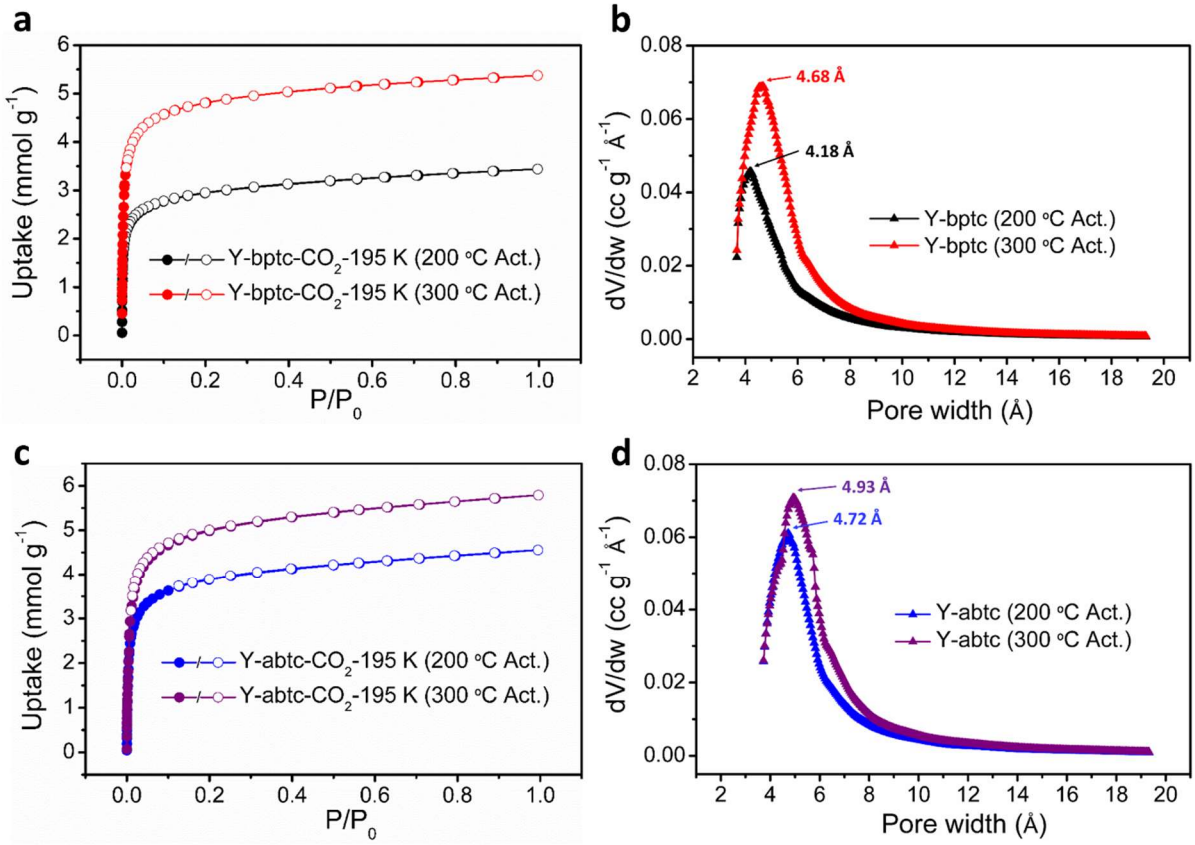

Figure 6. a) Adsorption-desorption isotherm of CO_2 at 195 K on Y-bptc activated at 200 and 300 °C and b) the corresponding pore size distribution. c) Adsorption-desorption isotherm of CO_2 at 195 K on Y-abtc activated at 200 and 300 °C and d) the corresponding pore size distribution.

A tailor-made microporous metal-organic framework designed through a topologically guided SBU replacement strategy exhibits the highest selectivity for fast and efficient separation of propane and propylene via size exclusion adsorption mechanism. This material, with excellent thermal and hydrothermal stability, facile and scalable synthesis, is capable of producing polymer-grade propylene (99.5%) from a typical propane/propylene mixture of cracking products.

metal-organic frameworks, adsorptive separation, olefin/paraffin separation, molecular sieving

Hao Wang, Xinglong Dong, Valentina Colombo, Qining Wang, Yanyao Liu, Wei Liu, Xin-Long Wang, Xiao-Ying Huang, Davide M. Proserpio, Angelo Sironi, Yu Han, and Jing Li*

Tailor-Made Microporous Metal-Organic Frameworks for the Full Separation of Propane from Propylene Through Selective Size Exclusion

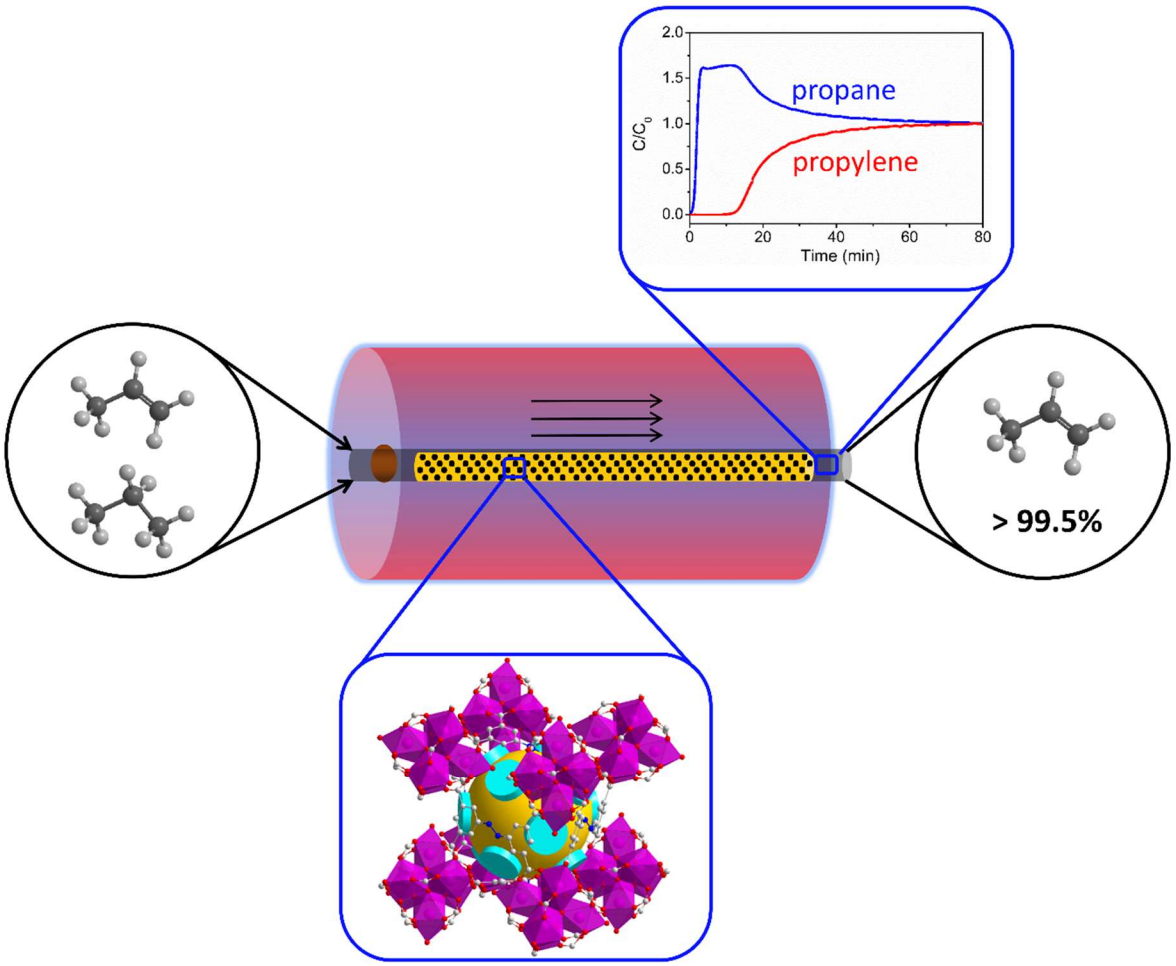

Copyright WILEY-VCH Verlag GmbH & Co. KGaA, 69469 Weinheim, Germany, 2016.

Supporting Information

Tailor-Made Microporous Metal-Organic Frameworks for the Full Separation of Propane from Propylene Through Selective Size Exclusion

*Hao Wang, Xinglong Dong, Valentina Colombo, Qining Wang, Yanyao Liu, Wei Liu, Xin-Long Wang, Xiao-Ying Huang, Davide M. Proserpio, Angelo Sironi, Yu Han, and Jing Li**

Experimental Details

General Information: All reagents were used as received unless otherwise specified. ^{1}H NMR data were collected on a 300 MHz Oxford NMR unit. X-ray single-crystal data collection of Y-bptc was obtained on a Bruker D8 Venture diffractometer equipped with a graphite monochromator using Mo Kα radiation (λ = 0.71073 Å) at 173 K. A multiscan technique was used to perform adsorption corrections. The crystal structure was solved using direct methods and refined using the full matrix least-squares method on F^2 with anisotropic thermal parameters for all non-hydrogen atoms using the SHELXL-2014 program. All hydrogen atoms were located in calculated positions and refined isotropically. Powder X-ray diffraction patterns were recorded on a Ultima IV with Cu Kα radiation (λ= 1.5406 Å). Data were collected at room temperature at 2θ = 3-40° with a scan speed of 2°/min and operating power of 40 kV and 44 mA. For structure solution process, PXRD data were collected on a Bruker AXS D8 Advance diffractometer (of the University of Milan, see next pharagraph). Thermogravimetric analysis was carried out on a Q5000 (TA Instruments) analyzer. For each run 3-4 mg of sample was heated from room temperature to 600 °C at a ramp rate of 10 °C/min. N_2 adsorption experiments at 77 K and CO_2 adsorption measurements at 195 K were performed on a Micromeritics 3Flex adsorption analyzer with liquid nitrogen and dry ice/ isopropanol as coolants, respectively. Prior to each measurement, ~ 100 mg of solvent exchanged sample was activated at 200 or 300 °C under dynamic vacuum overnight.

Thermodiffractomery: Variable-temperature X-ray powder diffraction (VT-PXRD) experiments were performed on Y-abtc. The experiment was carried out under N_2 flux by coupling a custom-made sample heater, assembled by Officina Elettrotecnica di Tenno, Ponte Arche, Italy, to the instrumental set-up described above. Powdered microcrystalline sample of Y-abtc was ground in an agate mortar and was deposited in the hollow of on a quartz zero-background plate framed by an aluminum skeleton. The data were acquired within a sensible, low-angle 2θ range (9-30°), heating the samples in situ in the temperature range RT-540 °C, with steps of 20 °C, under nitrogen flux. The N_2 atmosphere on the sample was insured by a home-made dome that fits on the sample holder and allow the X-rays to reach the sample through Kapton windows. Le Bail parametric refinements on the data measured in the range 30-540 °C (i.e. before a significant loss of crystallinity was observed) allowed describing the behavior of the unit cell parameters as a function of the temperature. The VT diffractograms and the results of the parametric data treatments are depicted in Supplementary Note 2. It should be noted that when comparing TGA and VTXRPD results, the reader must be aware that the thermocouple of the VT-PXPD set-up is not in direct contact with the sample, this determining a slight difference in the temperature at which the same event is detected by the two techniques. The TGA temperatures have to be considered as more reliable.

Hydrocarbon adsorption measurements: Hydrocarbon adsorption isotherms were collected with a volumetric gas sorption analyzer, Autosorb-1 (Quantachrome Instruments). Analysis temperature (25-80 °C) was controlled by a circulating-bath temperature controller. For a typical isotherm, around 150 mg of the solvent-exchanged sample was used and activated prior to data collection. Hydrocarbon adsorption rate measurements were performed on a gravimetric adsorption unit modified from a Q50 thermogravimetric analyzer (TA Instruments). For each measurement, ~ 20 mg of MOF sample was activated under nitrogen flow for 2 hours to remove any residual solvent. After cooling down to the adsorption temperature, hydrocarbon flow was mixed with the pure nitrogen stream and then introduced to the adsorption chamber mained at analysis temperature. Hydrocarbon partial pressure was controlled by adjusting the relative flow

rates of the two gas streams (pure nitrogen and pure hydrocarbon). Sample weight was recorded throughout the process which gives the information of the adsorbed amount of the adsorbate.
Column breakthrough experiments: Multicomponent column breakthrough experiments were conducted using a lab-scale fix-bed packed with the MOF sample. For a typical experiment, 0.53 g of MOF material was packed into a quartz column (5.8 mm I.D. ×150 mm) with silane treated glass wool filling the void space. A helium flow was used to for initial purging of the adsorbent. The MOF powder was activated at 200 °C overnight and the helium flow was then turned off while propane and propylene flows were introduced. Flow rates of each gas were adjusted to control the composition of the feed gas mixture. The effluent from the column was monitored using an online GC equipped with HP-PONA column and FID. The absolute adsorbed amount of gas i (*qi*) is calculated from the breakthrough curve by the equation:

$$q_i = \frac{F_i \times t_0 - V_{dead} - \int_0^{t_0} F_e \Delta t}{m}$$

Where Fi is the influent flow rate of the specific gas (cm^3/min); t_0 is the adsorption time (min); V_{dead} is the dead volume of the system (cm^3); F_e is the effluent flow rate of the specific gas (cm^3/min); and m is the mass of the sorbent (g).

Ab initio structure solution from powder XRD data: Gently ground powders of Y-abtc compound were deposited in the, 2 mm deep, hollow of a zero background plate (a properly misoriented quartz monocrystal). Diffraction experiments were performed at the University of Milan (Italy), using Cu-Kα radiation (λ = 1.5418 Å) on a vertical-scan Bruker AXS D8 Advance diffractometer in θ:θ mode, equipped with a Goebel Mirror and a linear Position Sensitive Detector (PSD), with the following optics: primary and secondary Soller slits, 2.3° and 2.5°, respectively; divergence slit, 0.1°; receiving slit, 2.82°. Generator setting: 40 kV, 40 mA. The nominal resolution for the present set-up is 0.08° 2θ (FWHM of the α1 component) for the LaB_6 peak at about 21.3° (2θ). The accurate diffraction patterns at RT and under nitrogen flow were acquired in the 5–105° 2θ range, with Δ2θ = 0.02° and exposure time 10 s/step with the same chamber used for the thermodiffraction experiment.

Structural analysis process. A standard peak search below 30° was followed by indexing through the singular value decomposition method, implemented in TOPAS, which led to a rhombohedral cell of approximate dimensions: a = 18.09 Å , b = 45.36 Å, c = 10.84Å and V = 12860 $Å^3$ (GOF(20) = 28.77). A Le Bail refinement of the pattern in *R*-3 gives rise to a slightly better R_{wp} than in *R*-3*c*. However, all peaks were already correctly described by the *R*-3*c* space group,. The slightly better fitting for *R*-3 is indeed simply due to the presence of unobserved peaks that contributes only to the modelling of the background. The determination of the background, correct unit cell parameters, sample displacement and profile parameters to be used in the subsequent simulated annealing runs, was indeed done on the basis of these structureless Le Bail refinements. The correctness of the *R*-3*c* space group was eventually confirmed by the successful two-step simulated annealing approach. Indeed, in the first run, we localized the $[Y_6(\mu_3\text{-}OH)_8]$ moiety, centred around a Wyckoff position *b*, and described by one Y and one O atom in general position and another O atom on a three-fold axis (Wyckoff site *c*). In the second step, we located the position of the abtc ligand, by using a flexible rigid body (Figure S7) consisting of the full ligand with halved occupancy, with its center of mass on a *d* Wyckoff site. Once confirmed to be the right position of the ligand, this was better described by half ligand with full occupancy. However, the obtained structural model, even if coherent for atom connectivity and for congruency with the Y-bptc cubic MOF, ended with a high R_{wp} = 30. We ascribed this to the high porosity of the Y-abtc MOF, in which the voids are, in the as synthesized form, filled by solvent molecules and dimethyl ammonium cations, that contributes to the overall intensity of the diffraction peaks. Indeed, to try to work on better data coming

from a partially activated sample, a first quick thermodiffraction experiment was performed, with heating steps of 50 °C from RT to 320 °C, under N_2 flux. The temperature was than kept at 320 °C for 5 hours and the powder was cooled to room temperature for a new overnight scan (by keeping the N_2 flux on the sample). The same structural model, refined on the new data set, reached a promising R_{wp} of 13.12. A subsequent Rietveld refinement with freely floating water oxygen atom, with a refinable site occupancy factor, revealed the presence of the oxygen of the coordinated water molecule (with occupancy 0.52) at the Y site. Moreover, the contemporary presence of residual electron density into the voids was described by freely roto-translating dummy C atoms, with refinable occupancy, with the aim of simulating the presence of the extra framework cations. This let to refine the powder diffraction pattern to a satisfactory R_{wp} = 11.41. During these Rietveld refinement steps, torsional angles around the C1-N1; C5-C8 and C3-C7 bonds were let to refinePeak shapes were described with the fundamental parameters approach and with the aid of 4th-order spherical harmonics. Moreover, the background was modelled by a Chebyshev polynomial function. The thermal effect was simulated by using a single isotropic parameter for the metal ion, augmented by 2.0 Å^2 for lighter atoms. The final Rietveld refinement plot are supplied in Figure S5. Crystal data are reported in the text. Fractional atomic coordinates are provided with the Supporting Information as CIF file.

Synthesis of H_4bptc

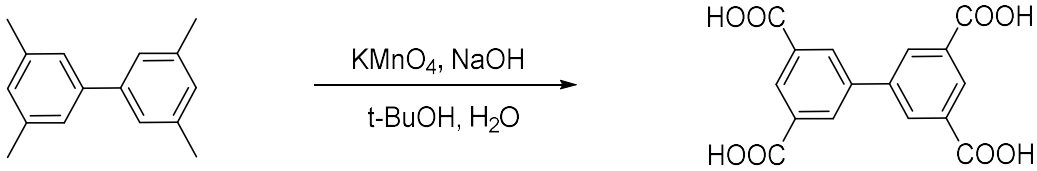

3,3'5,5'-tetramethylbiphenyl (5.0 g, 0.023 mol), NaOH (2.0 g, 0.05 mol) were mixed in t-BuOH/H_2O (100/100 mL) with stirring at 50 °C. $KMnO_4$ (43.0 g, 0.27 mol) was added in portions over one week. The temperature was subsequently increased to 70 °C and kept for 2 days. The mixture was filter when hot and the clear filtrate was added into 100 mL 6M HCl. White solid was obtained upon filtration. The crude product was recrystallized from DMF (~100 mL) to give pure H_4bptc with a yield 82%. ^{1}H NMR (400 MHz, DMSO-d^6): δ= 13.50 (4H, COOH), 8.51 (2H, Ar-H), 8.42 (4H, Ar-H).

Synthesis of H_4abtc

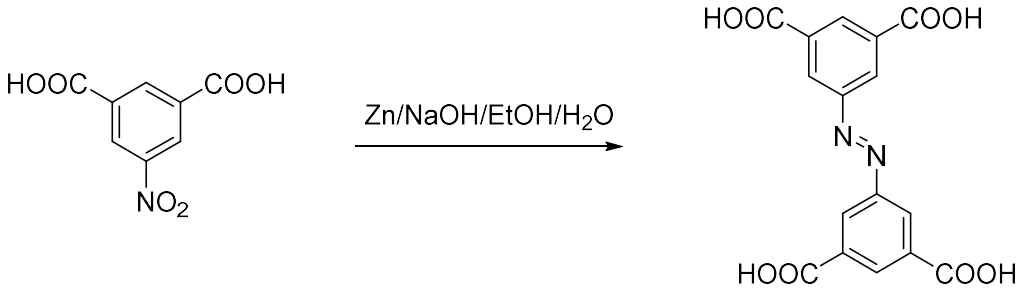

5-nitroisophthalic acid (2.1 g, 0.01 mol), NaOH (3.2 g, 0.08 mol), Zinc powder (2.1 g, 0.04 mol) were mixed in ethanol/H_2O (50/20 mL). The mixture was kept under refluxing for 12 hours before cooled to room temperature. Yellow solid was obtained through vacuum filtration which was then dissolved in 80 mL 1M NaOH solution. Upon filtration, the filtrate was acidified with 6 M HCl to get orange solid. The crude product was recrystallized from DMF to give pure H_4abtc as orange solid (1.3 g, yield: 73%). ^{1}H NMR (400 MHz, DMSO-d^6): δ= 13.38 (4H, COOH), 8.58-8.61 (6H, Ar-H).

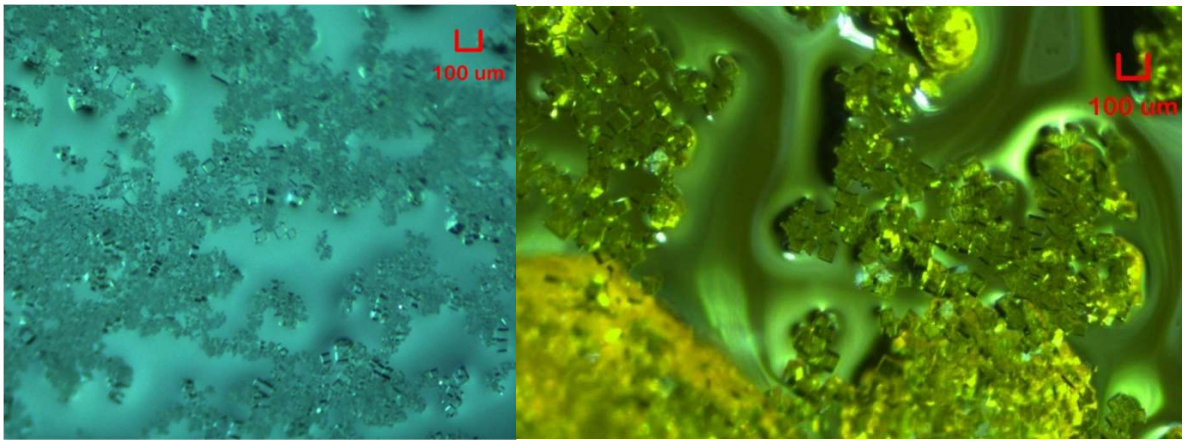

Figure S1. Microscopic images of crystals of Y-bptc (left) and Y-abtc (right).

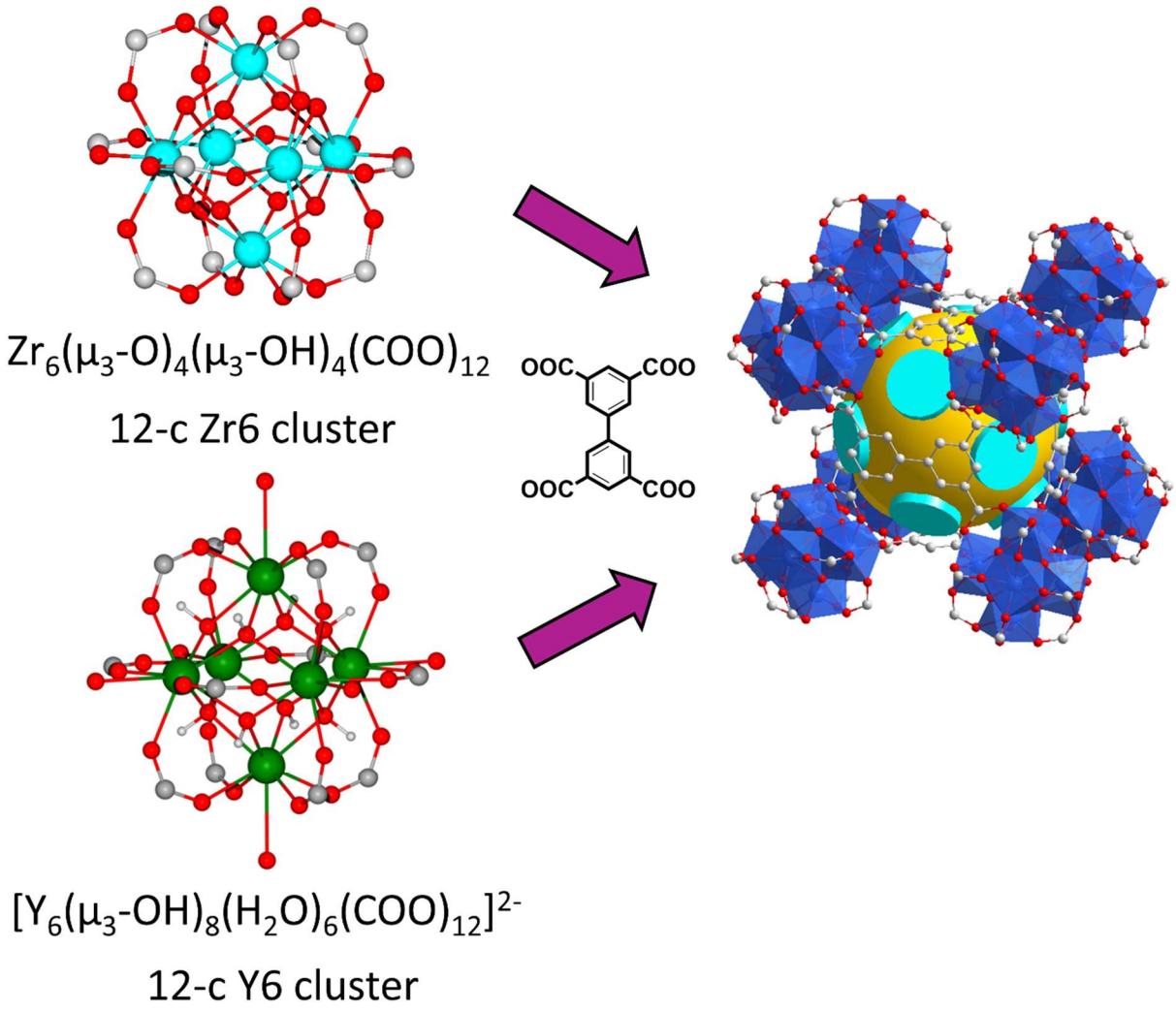

Figure S2. Comparison of Zr-bptc and Y-bptc. They are both built on 12-connected hexanuclear SBU and share similar connectivity and topology. But the two inorganic clusters are different in terms of composition and coordination.

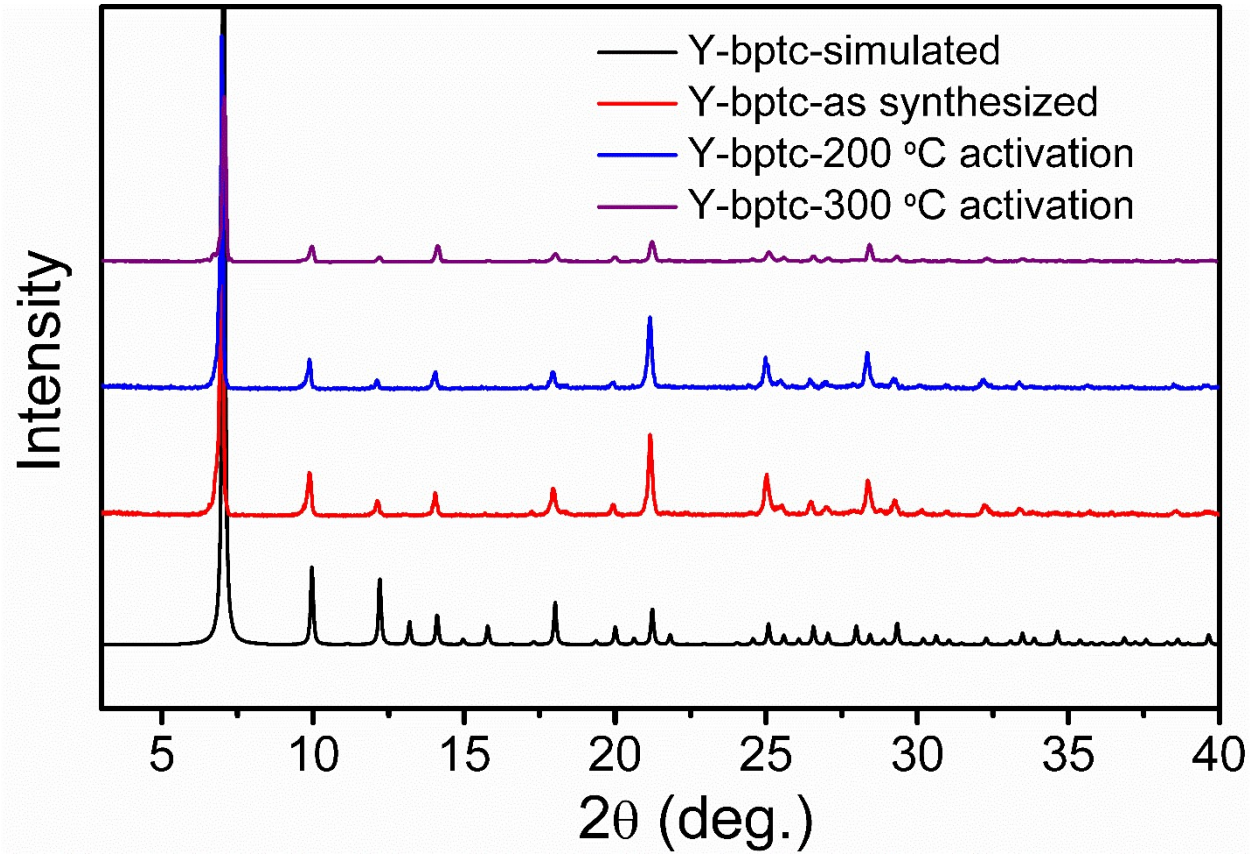

Figure S3 PXRD patterns for Y-bptc.

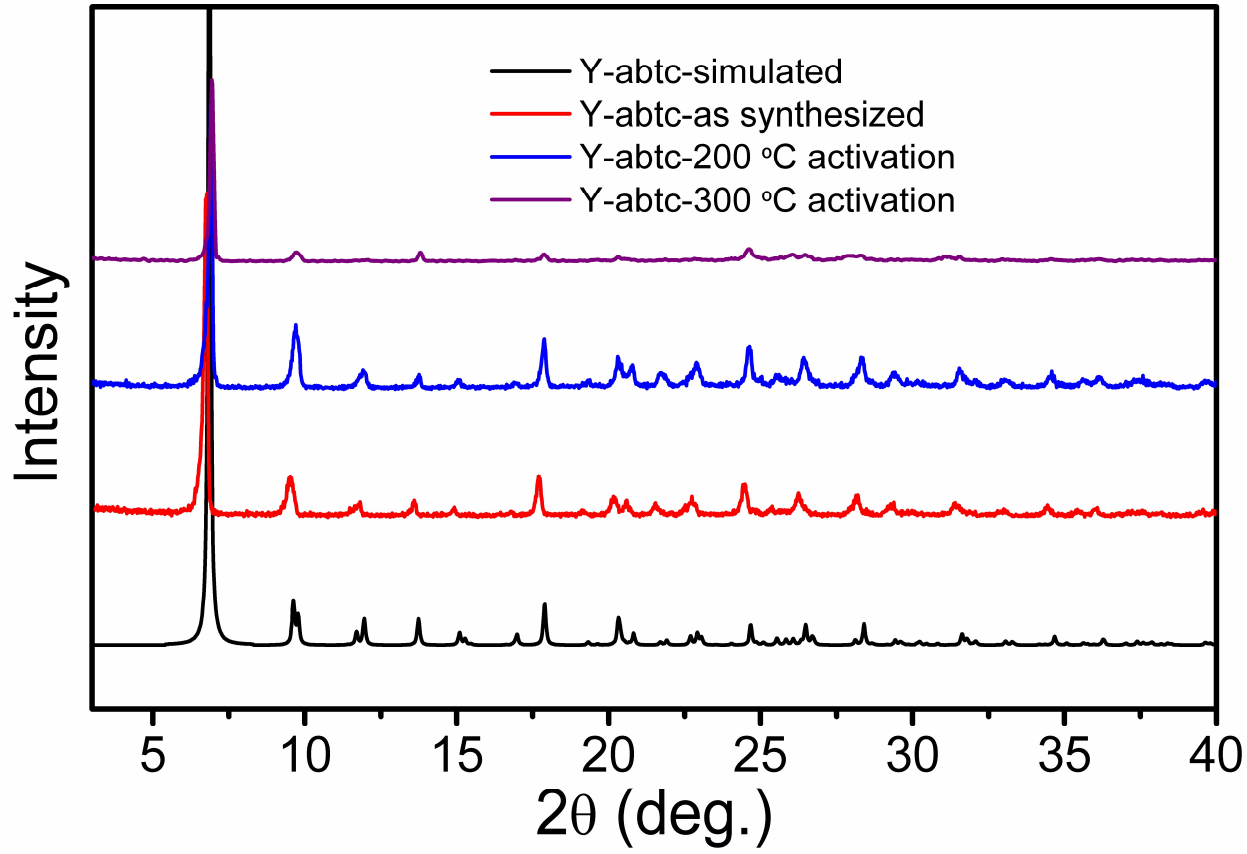

Figure S4. PXRD patterns for Y-abtc.

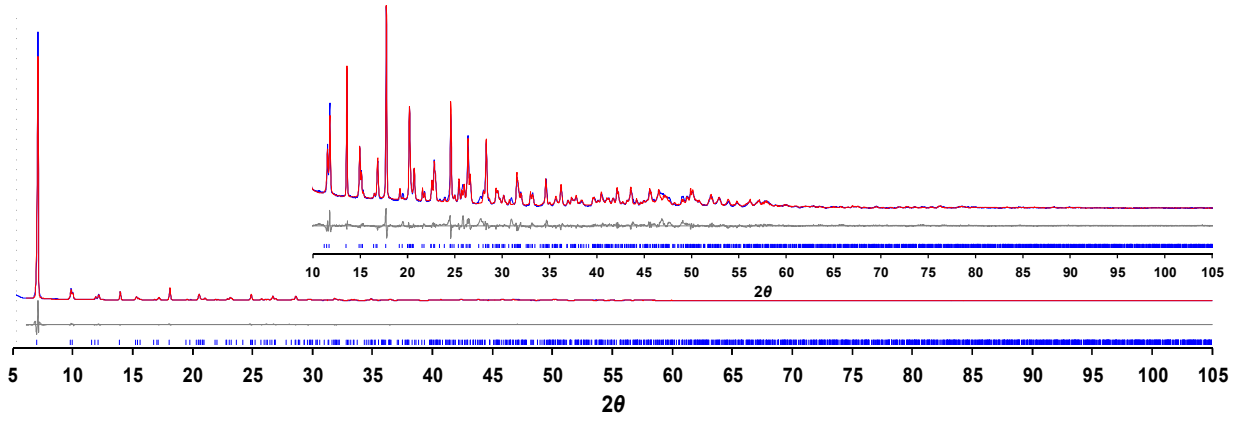

Figure S5. Final Rietveld Refinement plot for Y-abtc. Blue line, experimental data; red line, calculated; gray line, difference between experimental and calculated patterns. Blue tick marks represent peaks positions. The inset show a magnification of the high angle region. R_p and R_{wp} = 0.0754 and, 0.1022 for 5001 data collected in the 5–105° 2θ range. R_{Bragg} = 2.22.

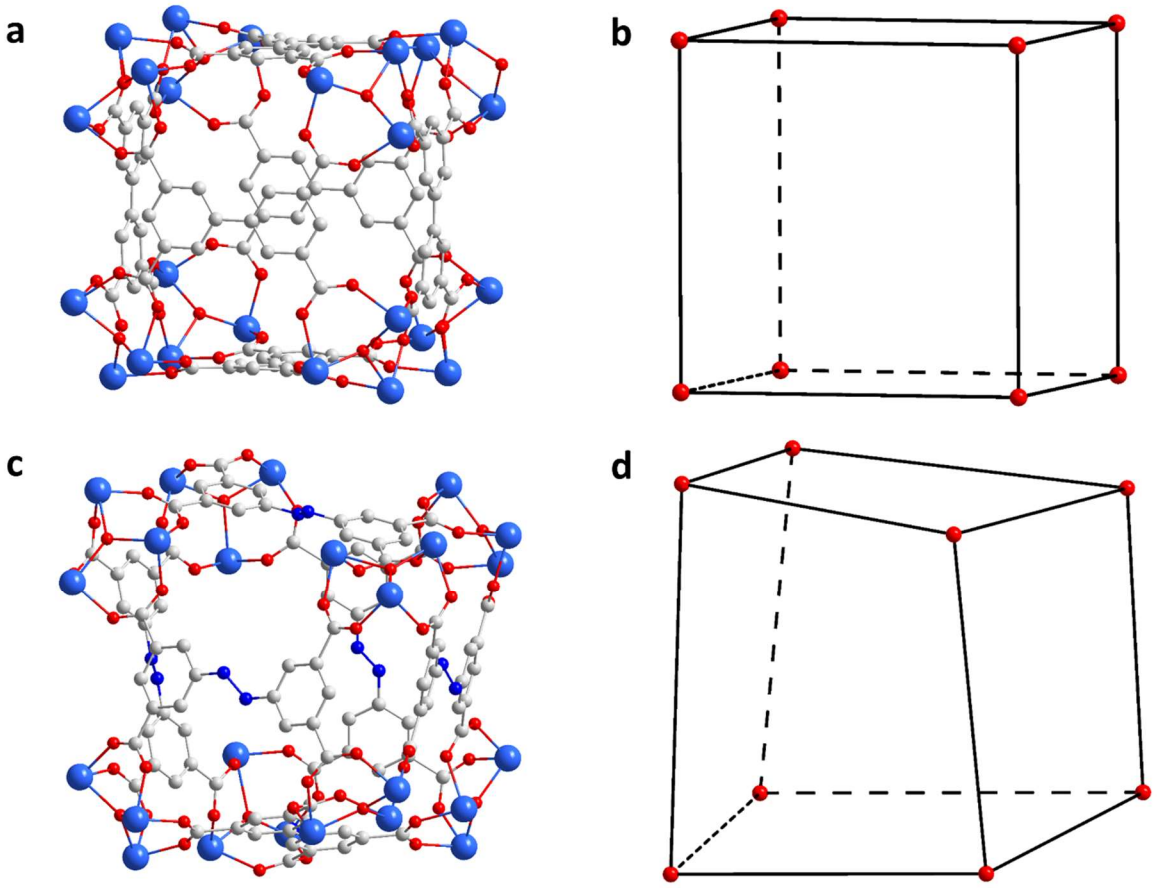

Figure S6. Crystal structure of a single cage and the shape of the cage depicted by connecting eight equivalent μ_3-O atom from the vertexes of the cage for Y-abtc (a, b) and Y-bptc (c, d).

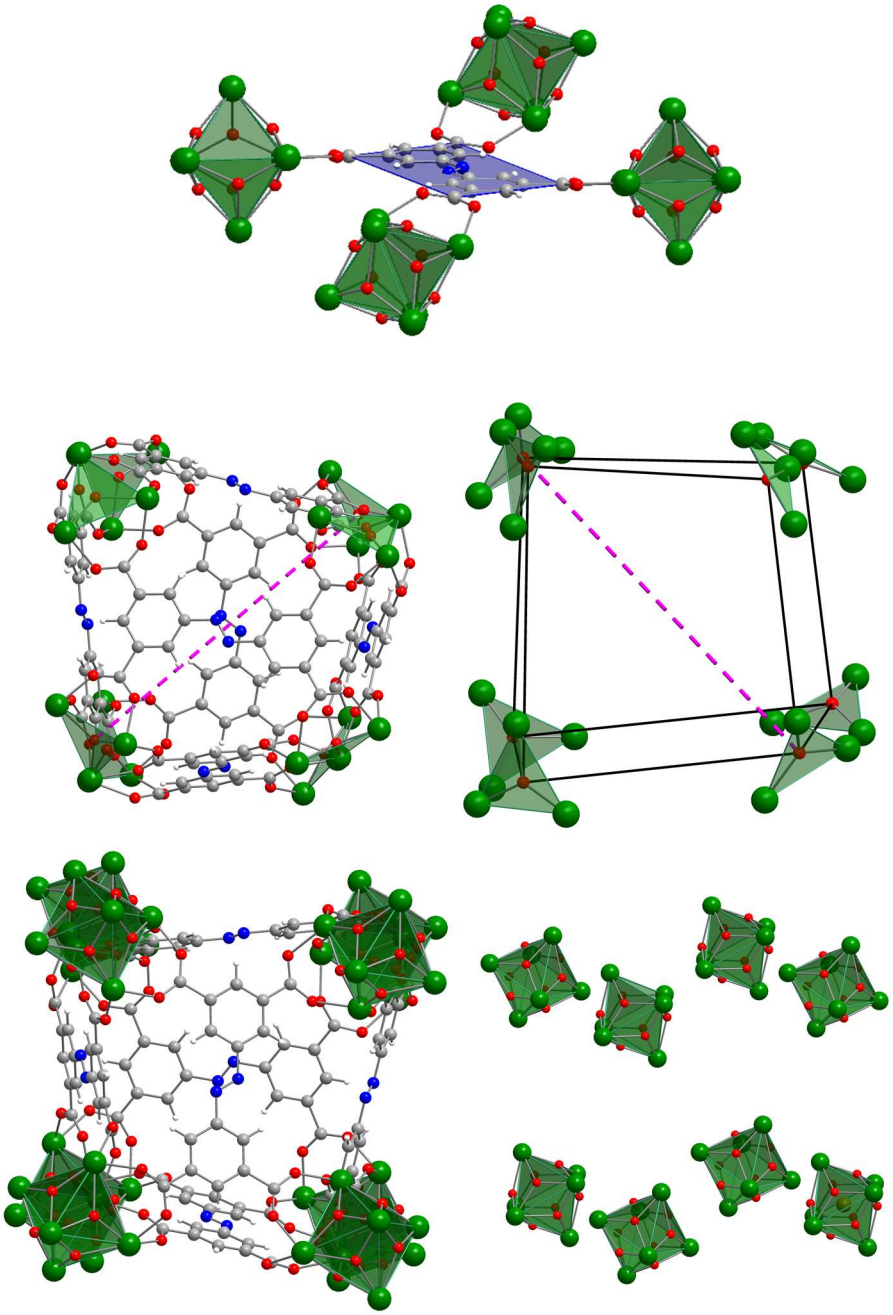

Figure S7. Coordination geometry of abtc and the distortion of the cages in Y-abtc. In this picture, the 3 fold axis is represented by the fragmented pink line.

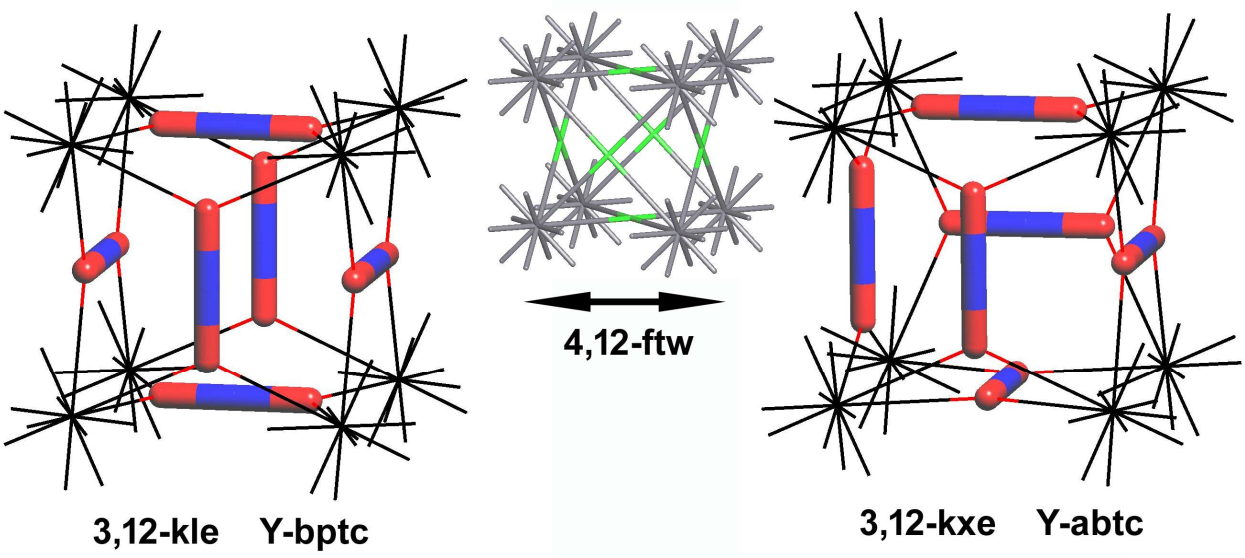

Figure S8. Comparison of 3,12-**kle** and 3,12-**kxe** nets derived from 4,12-**ftw**.

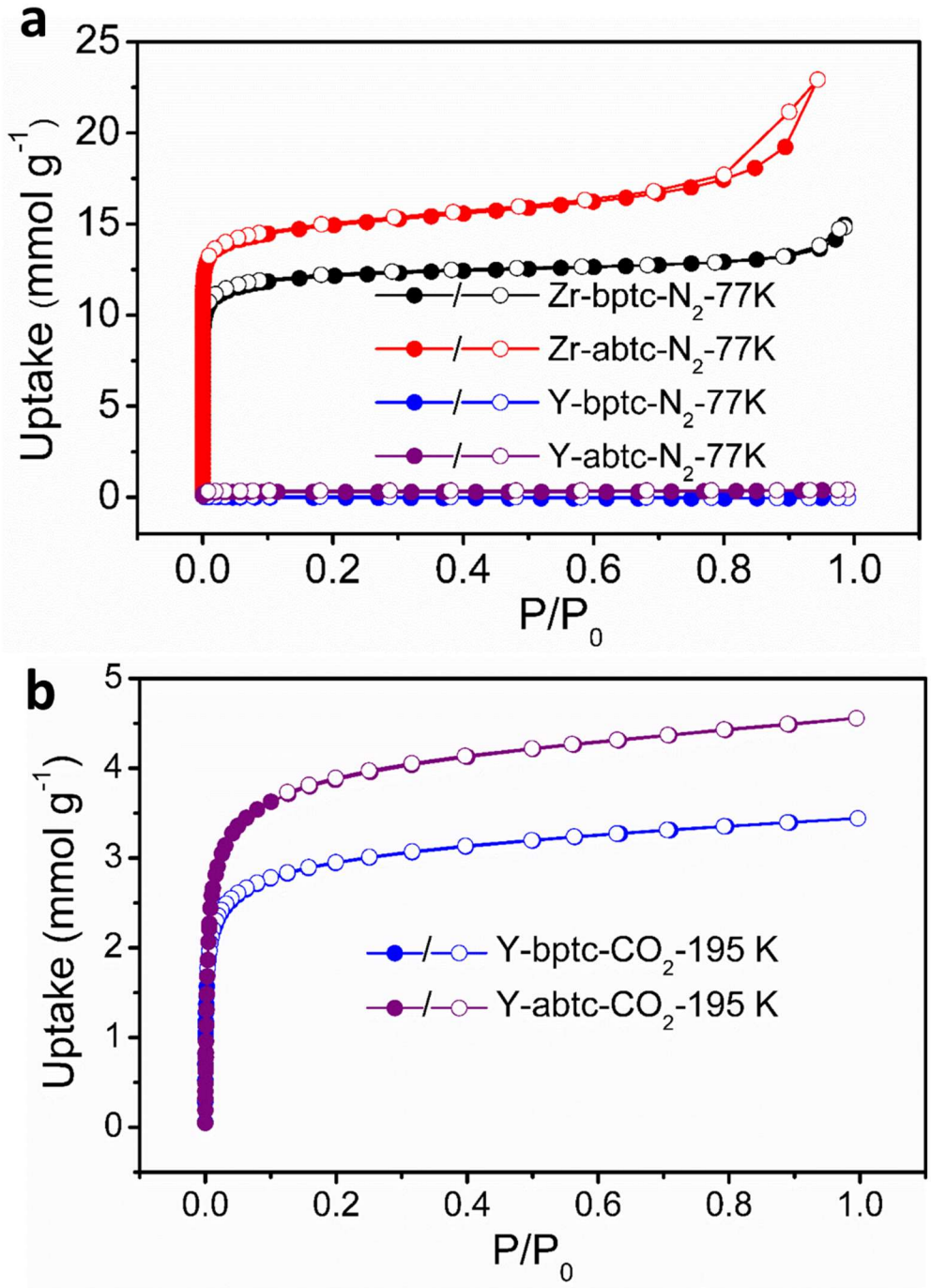

Figure S9. a) N_2 adsorption-desorption isotherms of Zr-bptc and Zr-abtc at 77 K. b) CO_2 adsorption-desorption isotherm of Y-bptc and Y-abtc at 195 K.

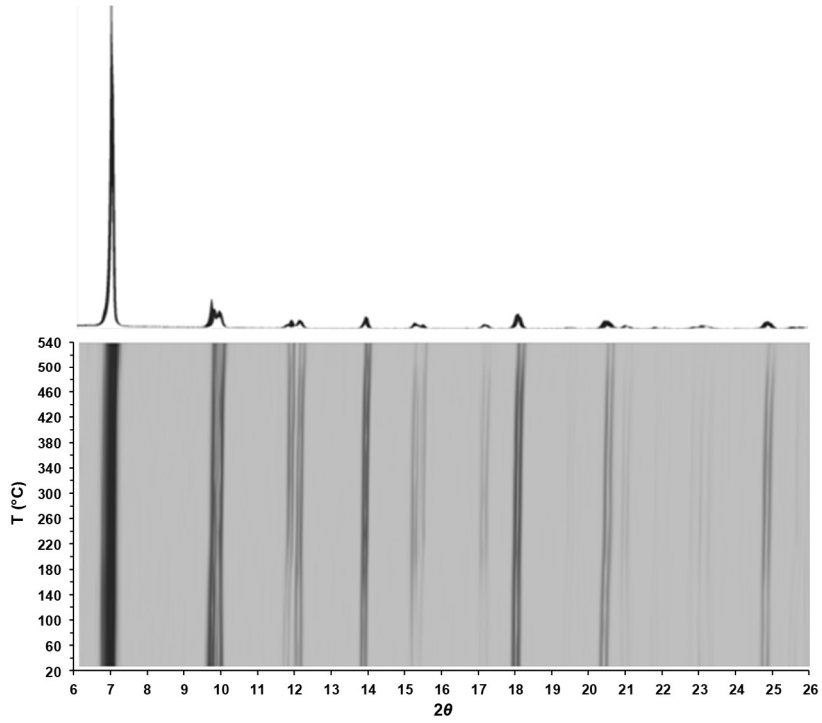

Figure S10. Head-on overlaid powder X-ray diffraction patterns measured at elevating temperatures in the range 20-540 °C for Y-abtc (top) and its two-dimensional contour plot as a function of 2θ and temperature (bottom), displaying the thermal stability. Notably, the diffraction patterns remained unaltered during the measurements except for minor changes in peak intensity.

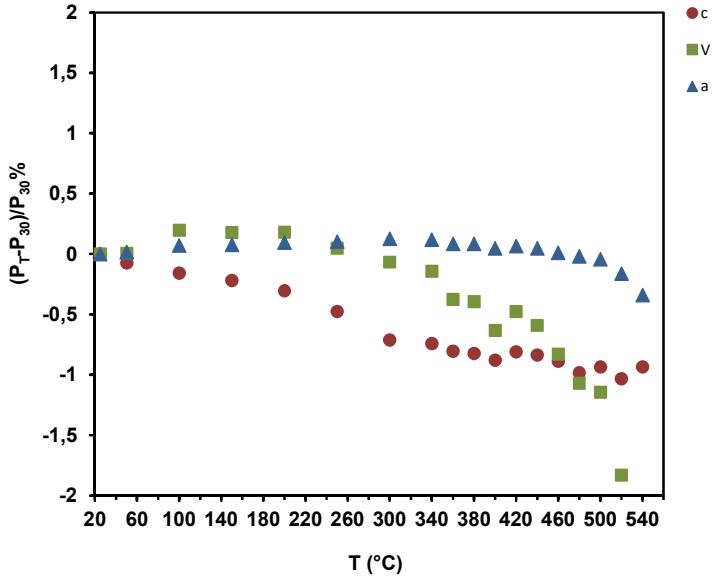

Figure S11. Variation of the unit cell parameters (P_T), normalized to the value at 30 °C (P_{30}), as a function of the temperature in the range 30-540 °C. **a**, blue triangles; **c**, red circles; **V**, green squares. This graph shows that the framework is substantially rigid, only a small (-2%) volume contraction is observed up to 520 °C (temperature at which the framework start losing its crystallinity).

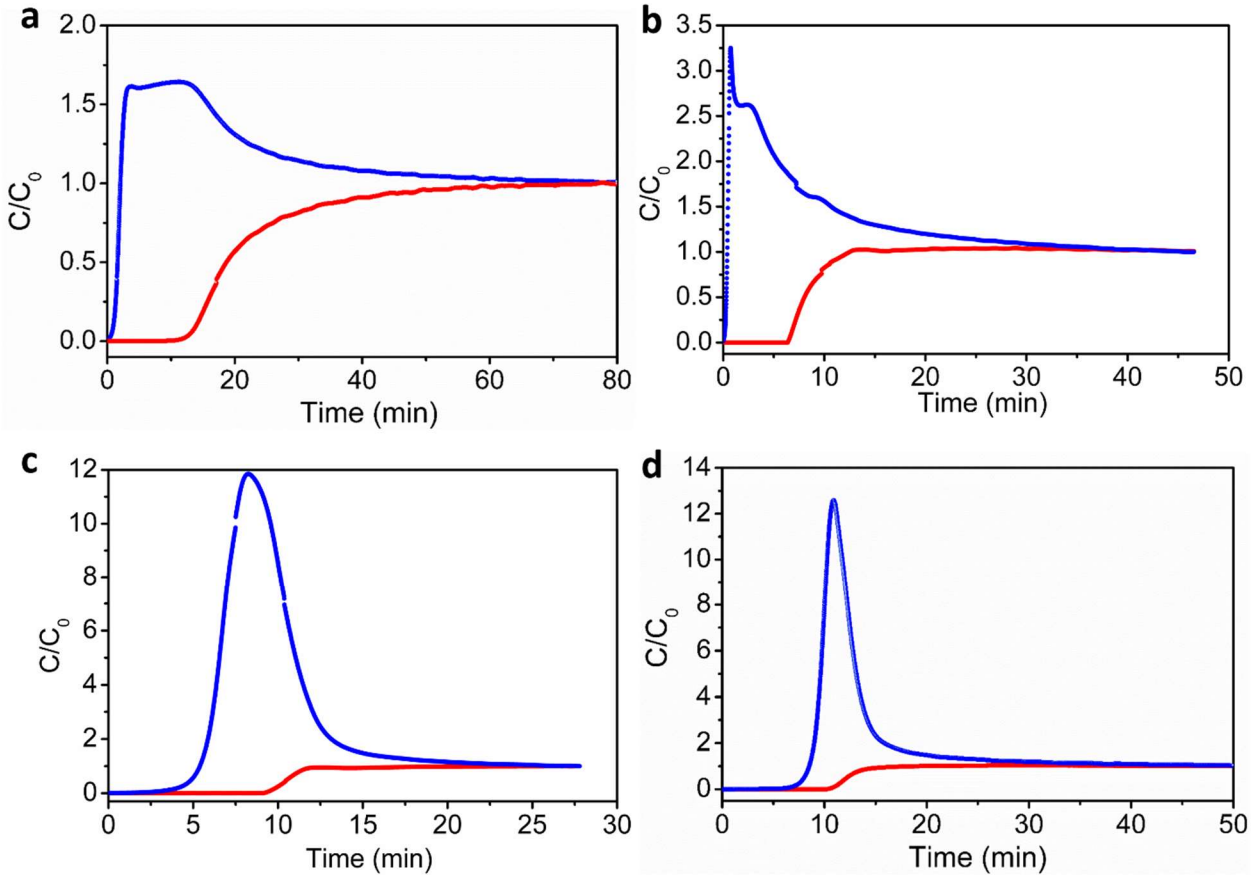

Figure S12. Breakthrough curves for binary mixtures of propane and propylene for a) propane: propylene = 50:50 (total flow rate: 1.6 cc min^{-1}), b) propane: propylene = 50:50 (total flow rate: 4 cc min^{-1}), c) propane: propylene = 10:90 (total flow rate: 1.6 cc min^{-1}), d) propane: propylene = 5:95 (total flow rate: 1.6 cc min^{-1})

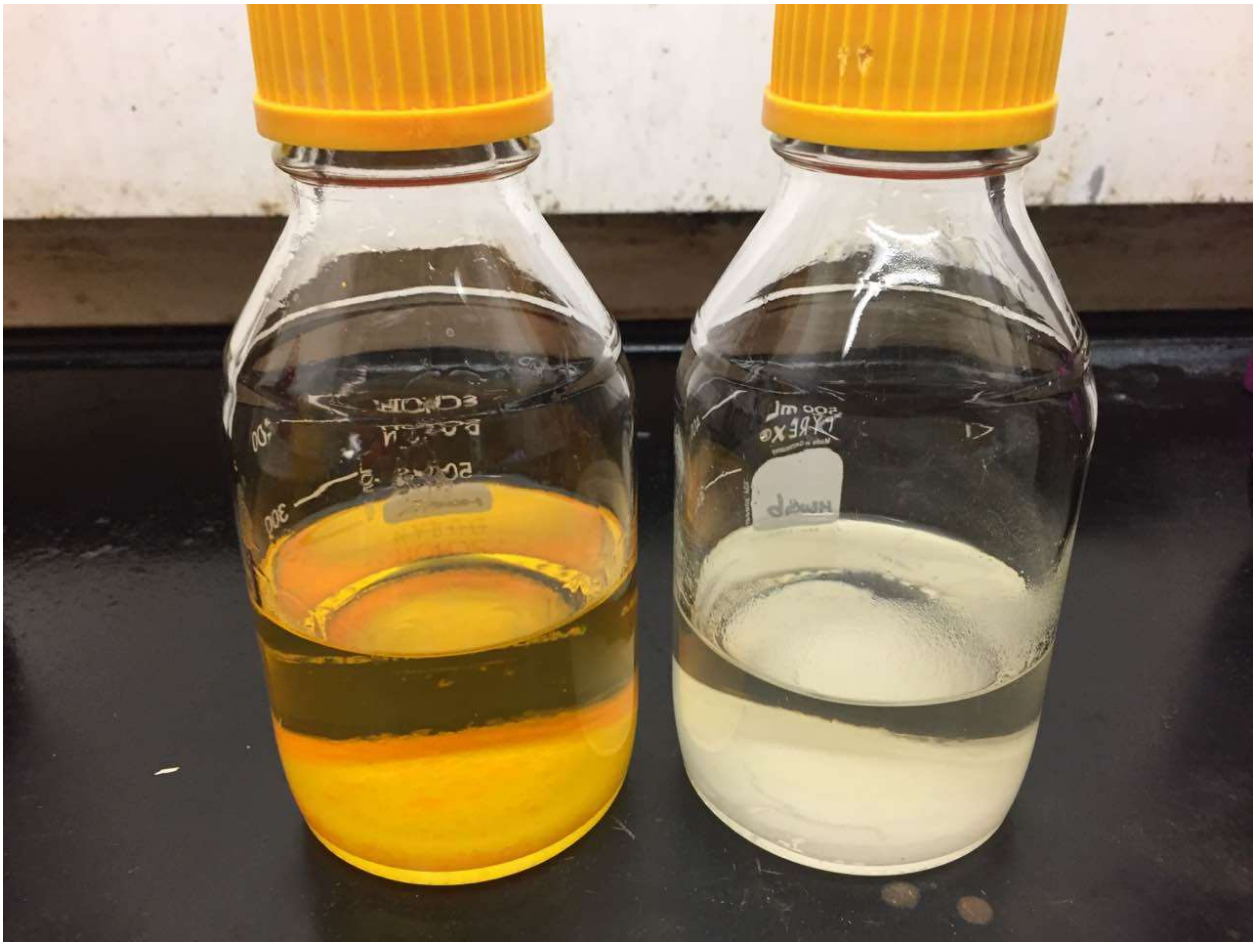

Figure S13. Gram scale synthesis of Y-abtc (left) and Y-bptc (right).

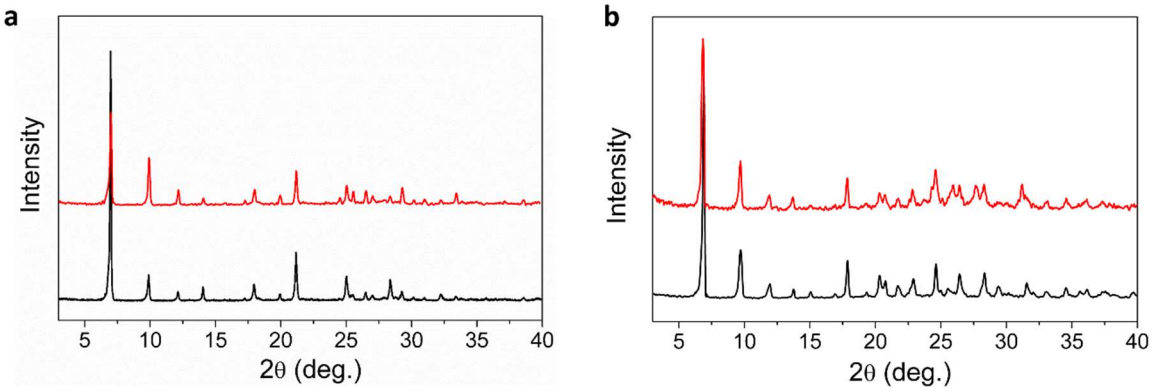

Figure S14. PXRD patterns of a) Y-bptc and b) Y-abtc synthesized with small scale (black, starting with 38.3 mg $Y(NO_3)_3 \cdot 6H_2O$) and 50× scaled up (red).

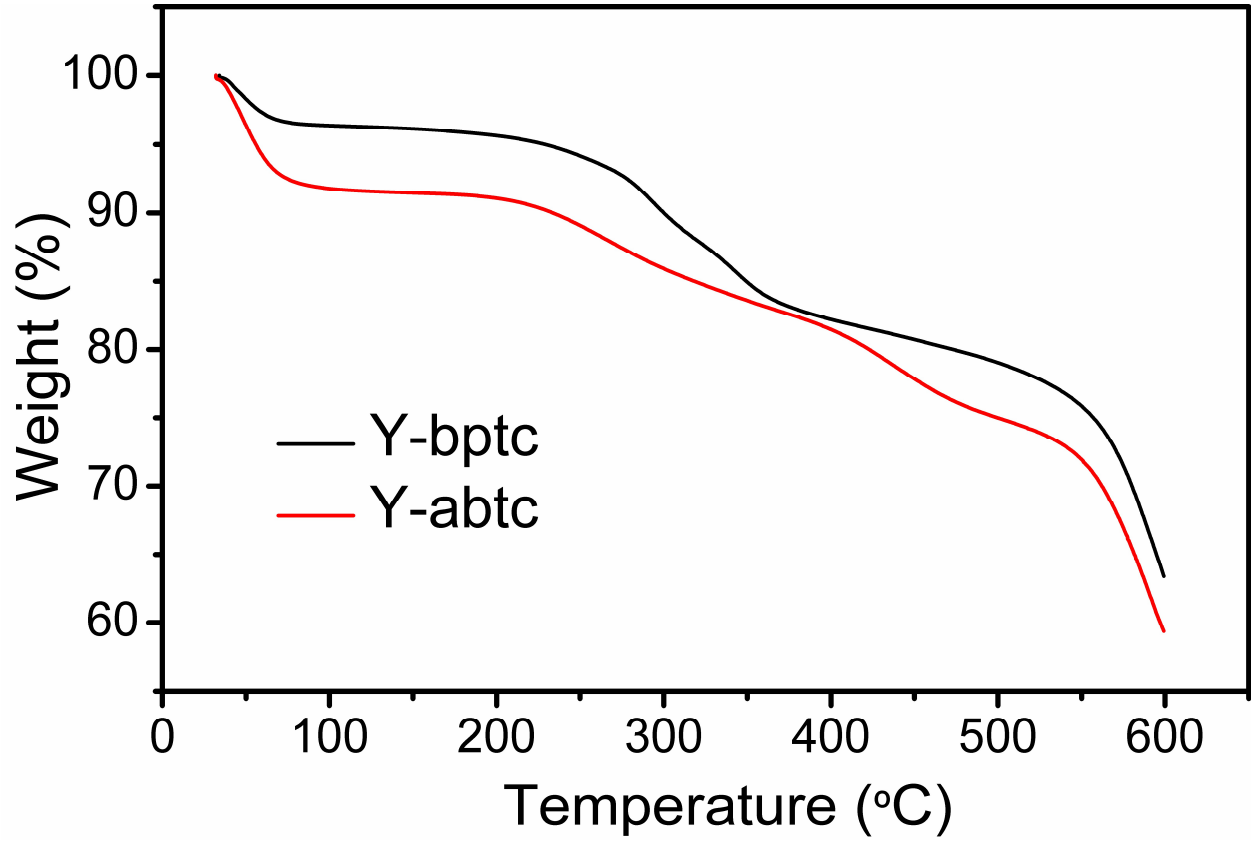

Figure S15. TGA curves for Y-bptc and Y-abtc.

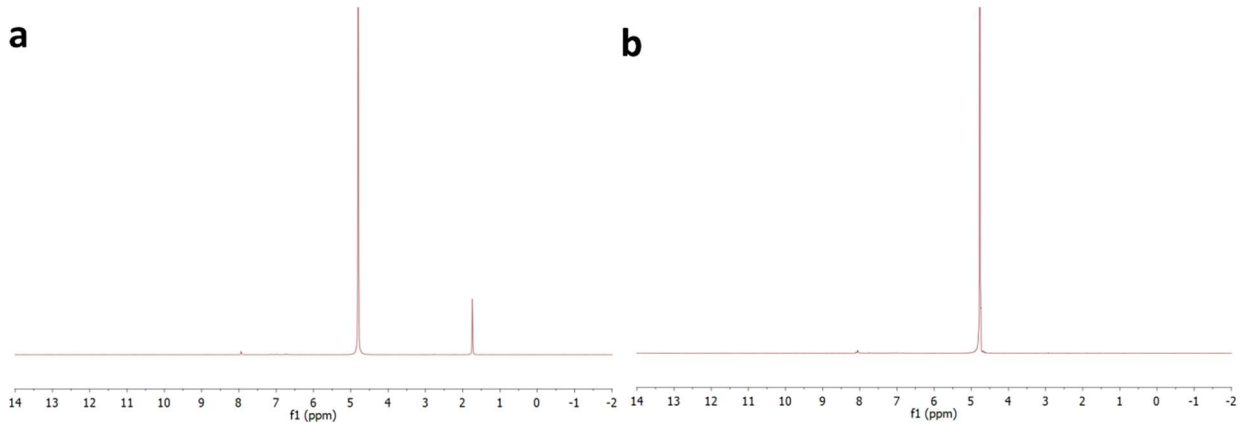

Figure S16. NMR spectra of base digested Y-abtc activated at a) 200 °C and b) 300 °C. The activated MOF was digested in NaOD (1 mmol/L in D_2O).

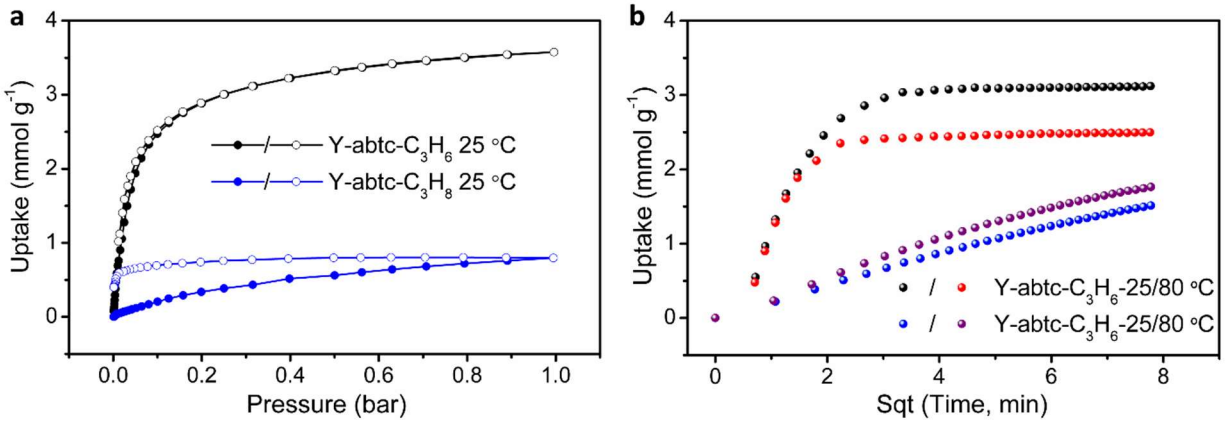

Figure S17. a) Adsorption isotherms and b) adsorption rates at 25 and 80 °C for Y-abtc activated at 300 °C.

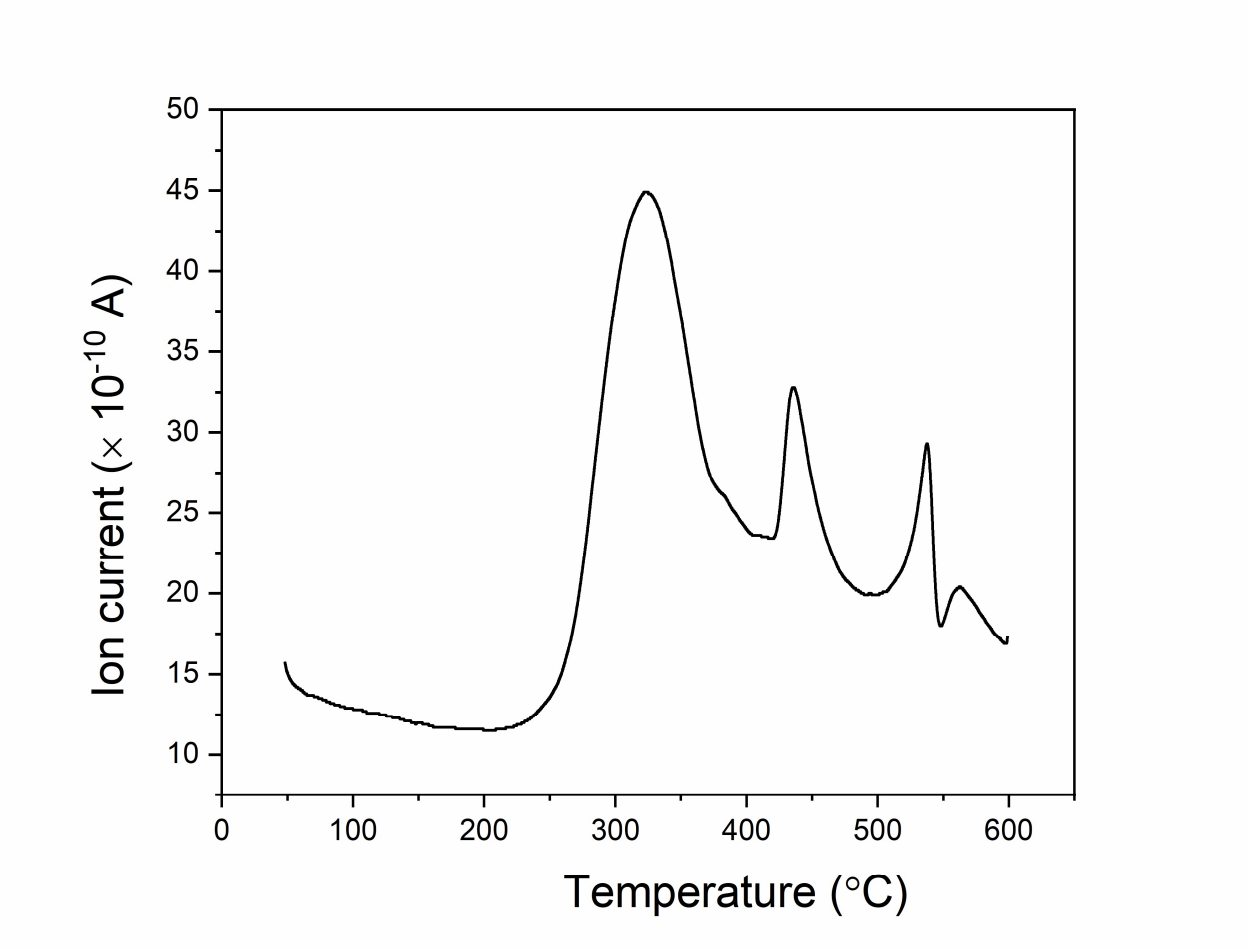

Figure S18. TG-MS spectrum for m= 45.